solvent content of the crystals, reducing the mosaicity and therefore increasing the diffraction quality of the crystals.

Four different dehydration methods were performed on the crystals using the same crystallization condition that resulted in the 3.9 Å structure (PEG 3350 and Na Malonate)[105]. Crystals from each method were screened on the home source. Method four, serial transfer of the cover slip, had the greatest increase in resolution in addition to being the easiest and most gentle method. Crystals were generated using this method with varying concentrations of precipitant in the reservoir (5-25%). Nine pucks containing 16 crystals in each puck were screened at the synchrotron at GM/CA Argonne. Only one crystal, the same crystal that was generated in the first attempt of this method, diffracted to a resolution of 2.69 Å. Dehydration resulted in a 14% decrease in the unit cell size (7,315,088$Å^3$ to 66,312,048 $Å^3$) resulting in an increase in resolution increasing the number of unique reflections 2.5 fold (33,660 to 87,354).

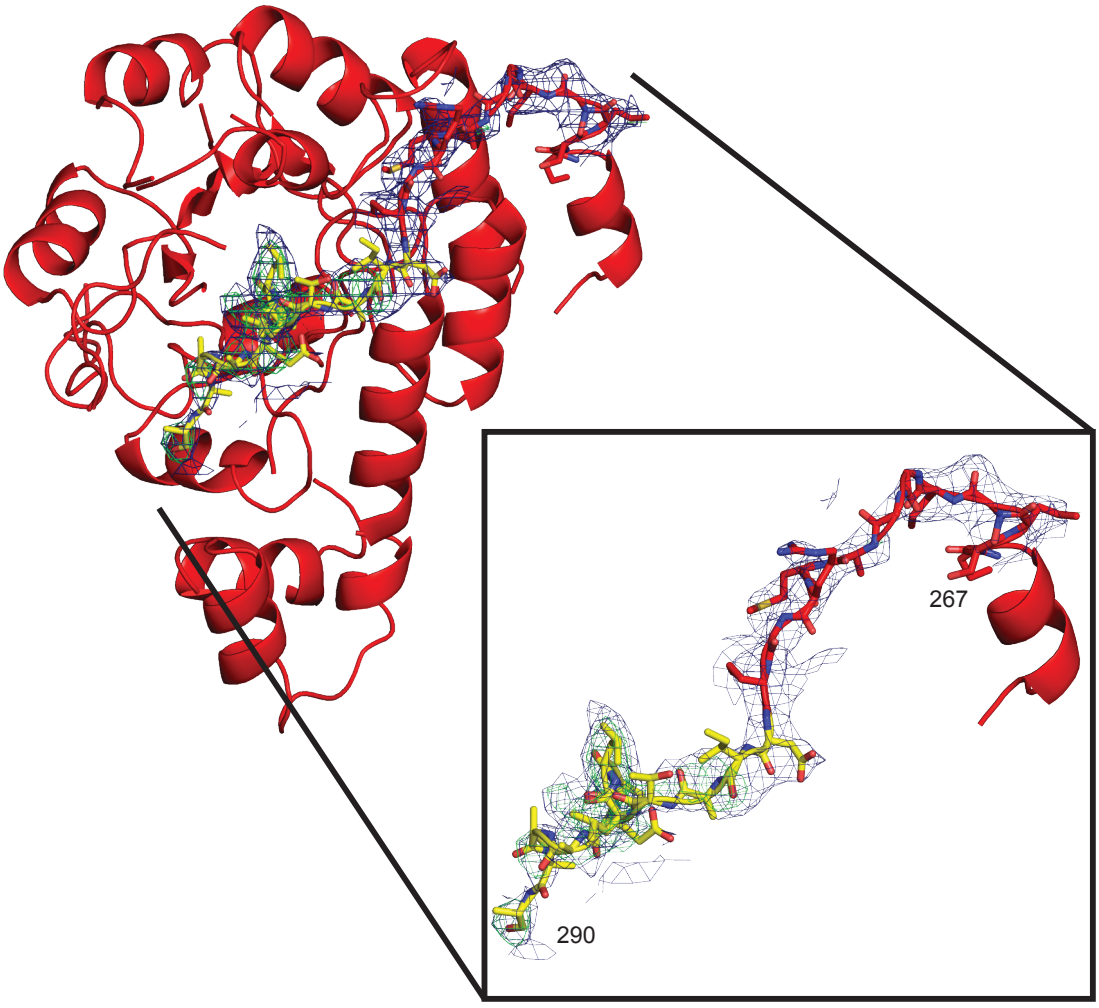

Figure 3.5 Initial crystals of PLPS/H169N$_T$/R5P/Gln diffracted to 4 Å, density for the C-terminal tail (yellow sticks) was present for the backbone to residue 290 ($2F_o$-F_c omit density contoured at 1 σ; blue, F_o-F_c omit density contoured at 3 σ; green).

Table 3:6 Data collection statistics for the 3.9 Å structure of PLPS/H169N$_T$/R5P/Gln.

PLPS/H169N$_T$/R5P/Gln	
Diffraction data	
X-ray Source	APS 23ID-D
wavelength	1.033
space group	$C222_1$
unit cell parameters (Å)	152.8, 255.5, 187.3
α, β, γ (°)	90, 90, 90
asymmetric unit	6 PdxS, 6 PdxT H169N
resolution limit (Å)	3.9 (4.04-3.9)
measured reflections	1424607
unique reflections	33660
avg. I/σ_I	22.9(4.37)
avg. redundancy	7.2(7.4)
completeness (%)	99.8(99.6)
R_{sym}	0.104(0.517)

Structure of PLPS with amino ketone and γ-glutamyl thioester covalent adducts

I obtained a crystal structure of intact PLPS ($PdxS_{12}PdxT_{12}$) with two covalent intermediates, the glutamate thioester of Cys78 in the glutaminase subunit (PdxT) and the R5P adduct at Lys81 in the synthase subunit (PdxS). The crystal structure of the double covalent intermediate trapped PdxS in a closed conformation and is highly informative about conformational changes that occur during the catalytic cycle (Fig. 3.6).

The glutamate thioester intermediate at the nucleophilic Cys78 was stabilized by creating a PdxT variant in which Asn was substituted for His169 in the catalytic triad (Fig. 3.7)[9]. The thioester appears at full occupancy all six PdxT subunits in the crystallographic asymmetric unit, as does the intermediate at PdxS Lys81 through the R5P C1 atom (Fig. 3.8). Thus, the synthase active site is poised to receive ammonia. Formation of this synthase state apparently required both the glutaminase subunit

(PdxT) and also catalysis in its active site, *i.e*. formation of the glutamate thioester intermediate. PdxS structural differences relative to the *G. stearothermophilus* PdxS-only structures[48] (Chapter 2), a *B. subtilis* intact PLPS structure[9] and a *T. maritima* intact PLPS[49] are limited to the synthase active site; there appear to be no changes in subunit contacts. Similarly, the glutaminase active site and subunit exhibit no changes relative to the *B. subtilis* PLPS structure with the glutamate thioester intermediate[9]. Interaction of PdxT with PdxS sequesters the glutaminase active site from bulk solvent, in a manner that would slow the loss of labile ammonia generated in the glutaminase reaction. The ammonia generation site faces the entrance to the PdxS β_8/α_8 barrel at the opposite end from the synthase active site. The hydrophobic barrel interior is suited to diffusion of uncharged ammonia to the synthase active site.

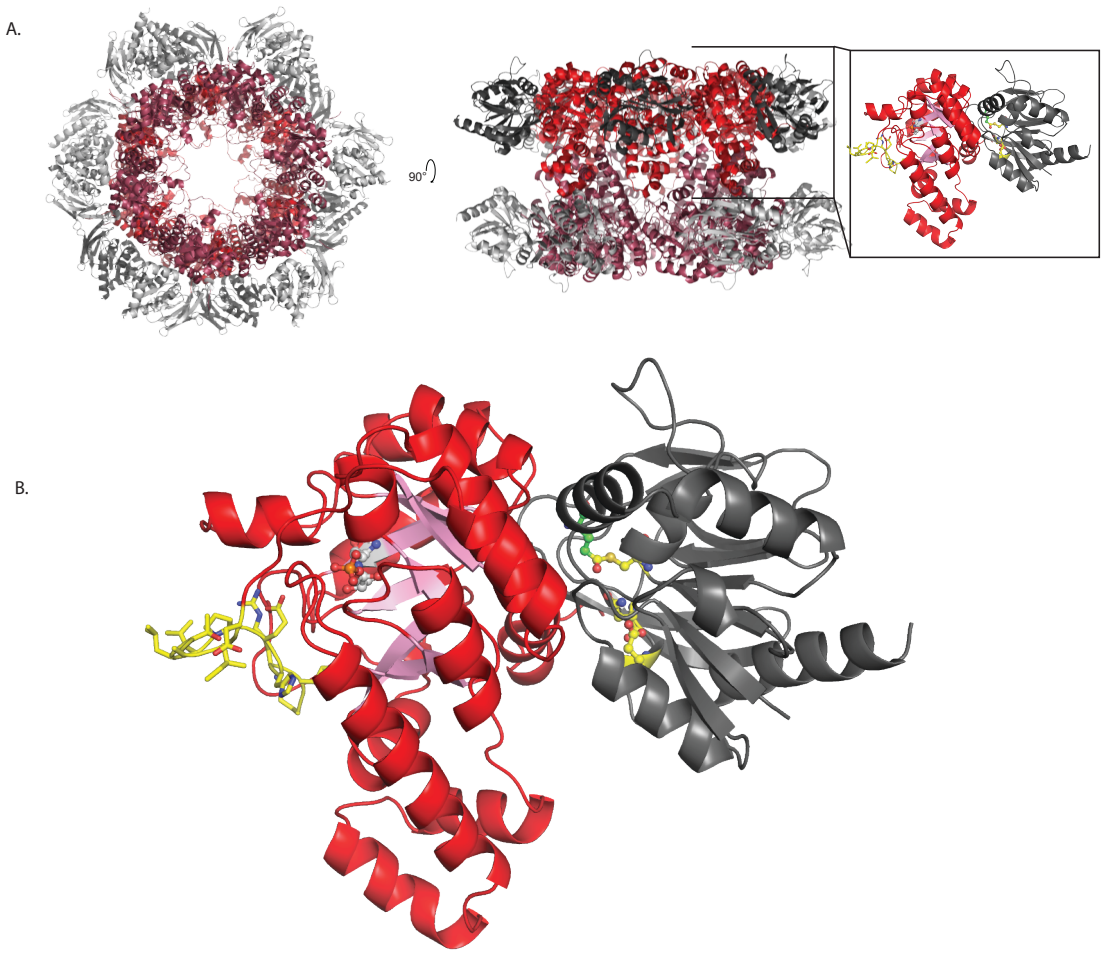

Figure 3.6 PLPS overall architecture. A. The 24-subunit complex of PLPS (12 PdxS (red and dark pink) and 12 PdxT (light gray and dark gray)). The catalytic triad of PdxT is shown in yellow ball-and-sticks. Glutamine is show in green ball-and-sticks. The Lys81/R5P adduct shown in gray ball-and-sticks. The ordered C-terminal tail of PdxS is shown in yellow sticks. B. A close up of the catalytic protomer of PLPS (1 PdxS (red): 1 PdxT (gray)). The β-strands of PdxS are shown in light pink.

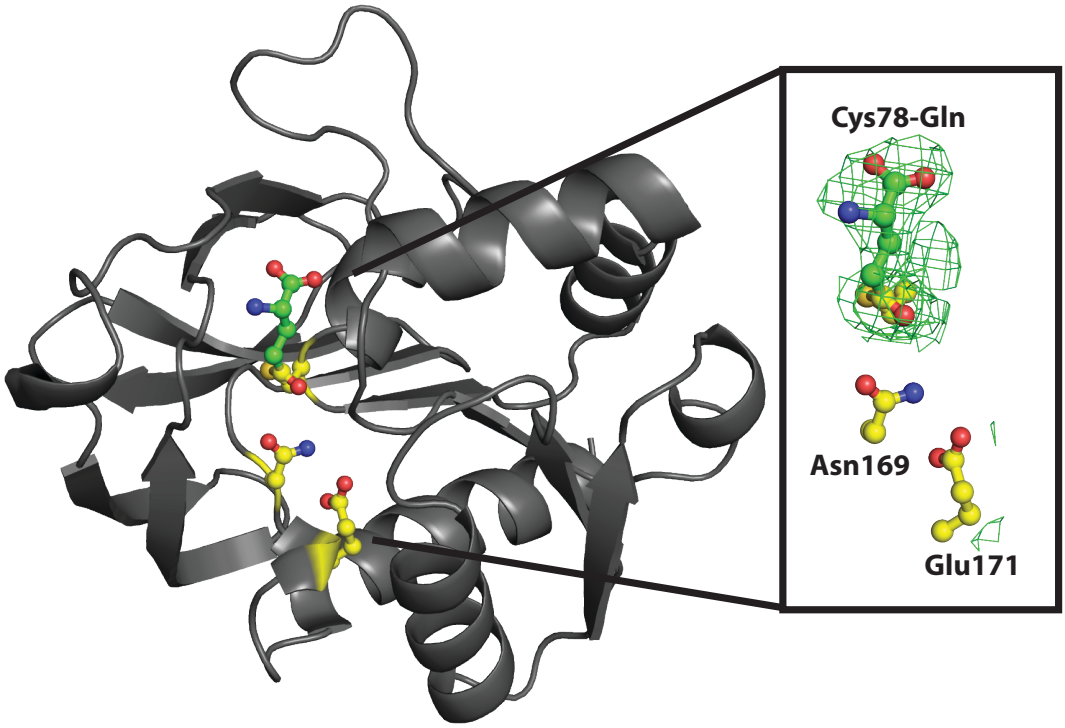

Figure 3.7 The mutated form of PdxT (H169N) traps the glutamyl-thioester intermediate. Continuous density (green; F_o-F_c omit density contoured at 2.5 σ) is present for the covalent bond between glutamine (green, ball-and-sticks) and the nucleophilic cysteine (yellow, ball-and-sticks).

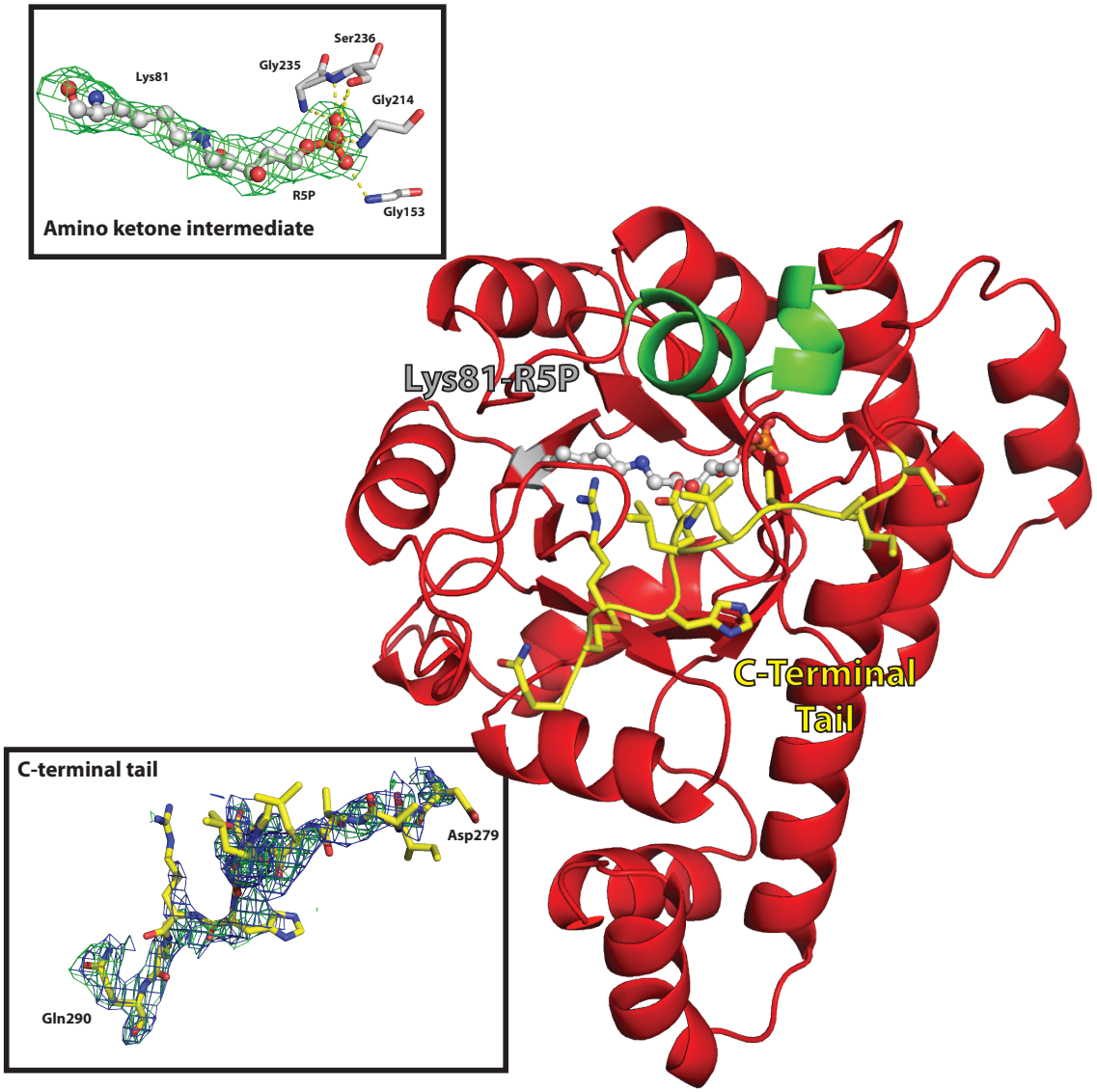

Figure 3.8 Double covalent intermediate orders the C-terminal tail. The C-terminal tail (yellow; F_o-F_c omit density contoured at 3 σ, blue; 2F_o-F_c omit density contoured at 1 σ) of PdxS is ordered with the exception of the last four residues. The amino ketone adduct between Lys81 and R5P (blue; F_o-F_c omit density contoured at 2.5 σ).

In contrast to the glutaminase active site, the synthase active site of the PLPS double covalent intermediate reflects a remarkable set of conformational changes relative to previous structures of *G. stearothermophilus* PdxS. These changes

sequester the site from bulk solvent and provide more specific contacts with the R5P covalent intermediate (Fig. 3.9). Three elements of the synthase structure are changed. Most dramatically, the C-terminal tail is ordered from residue 272-290, leaving only residues 291-294 without electron density. Second, an internal peptide (residues 49-56) becomes ordered and forms a short helix (α2a, residues 48-54) over the active site. Finally, helix α8' (236-240) shifts 3 Å towards the phosphate group of the covalent intermediate. These structural elements meet at the synthase active site and interact with one another.

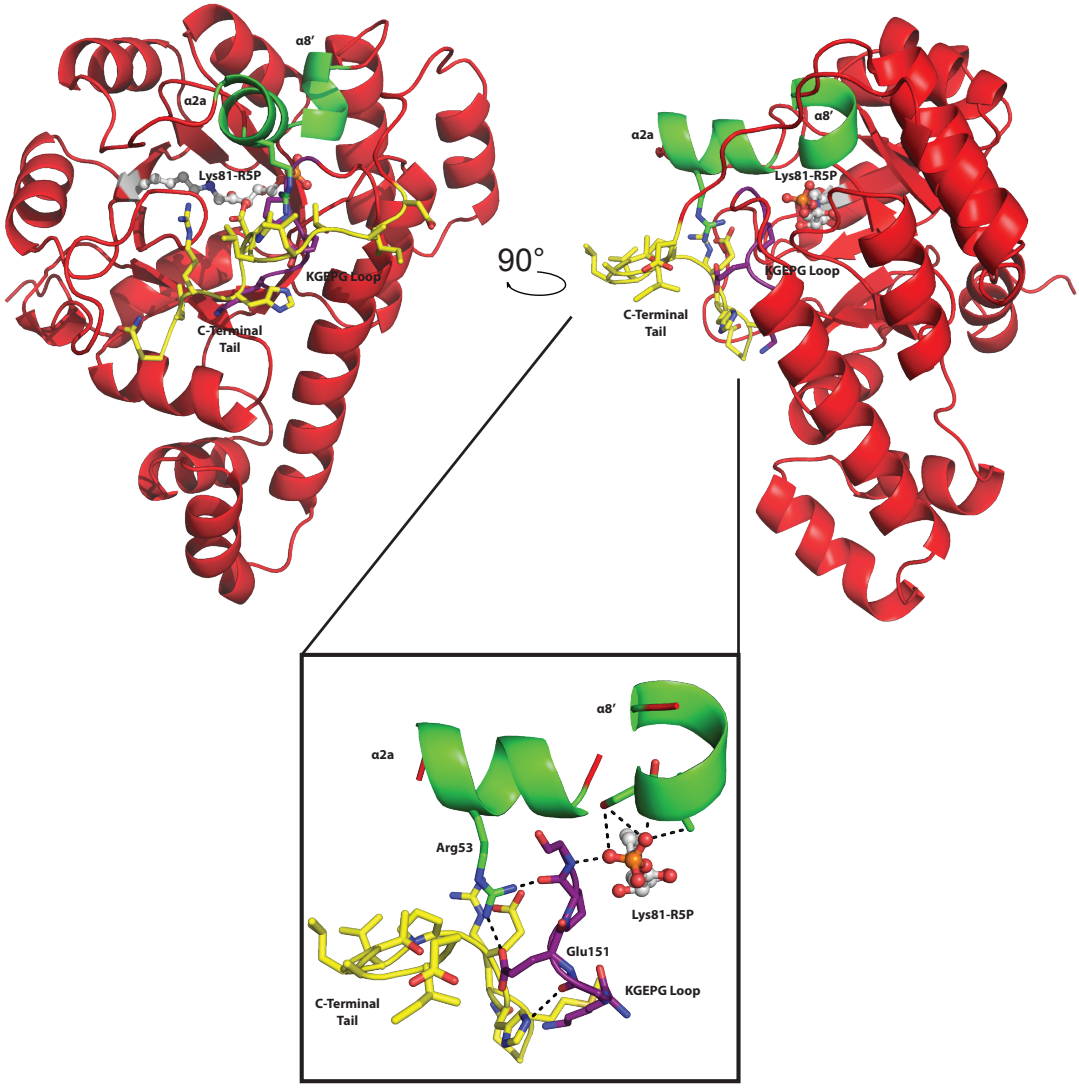

Figure 3.9 PdxS is in a closed conformation. Conserved structural elements bury the amino ketone intermediate into the core of PdxS (helices α2a and α8'; green, KGEPG; purple/sticks, C-terminal tail; yellow/sticks).

The shift of helix α8' brings backbone amides at its N-terminus (Gly235 and Ser236) within hydrogen bonding distance of the phosphate of the covalent intermediate. The phosphate is thus enclosed by α8' and the loops containing Gly153 and Gly214, which also form hydrogen bonds with phosphate oxygens. An additional hydrogen bond

is formed with the Ser236 side chain. The shifted position of helix α8' is stabilized by the formation of helix α2a, which delivers the invariant Arg53 side chain to the active site where it stabilizes the phosphate enclosure through hydrogen bonds with the Glu151 side chain and the Pro152 backbone carbonyl group (Fig. 3.9). The conserved "KGEPG" loop (residues Lys149 - Gly153) is central to this closure of the active site through interactions with phosphate and with Arg53. The KEGPG loop is the only structural element that interacts directly with the covalent intermediate, helix α2a and the C-terminal tail. Substitutions were made to disrupt the interaction between helix α2a (Arg53) and the KGEPG loop (Glu151) (Table 3.7). The initial velocity of chromophore formation decreased significantly in comparison to the initial velocity of PLP synthesis. However, glutaminase activity was not significantly affected (Fig. 3.10).

Table 3:7 Initial velocity as percent wild type for PdxS variants.

PdxS Variant	Chromophore Formation (initial velocity as % WT)	PLP Synthesis (initial velocity as % WT)
R53E	33 ± 0.4	29 ± 0.6
R53K	10 ± 0.7	41 ± 2.6
R53Q	1 ± 0.4	8 ± 1.6
R53A	3 ± 0.3	16 ± 1
E151Q	6 ± 0.6	36 ± 2.8
E151S	8 ± 1.3	51 ± 1.8
E151A	15 ± 0.2	55 ± 1.6
E291D	80 ± 3	85 ± 3.8
E291Q	69 ± 1.7	64 ± 2
E291A	72 ± 2	61 ± 5.6
R292K	23 ± 1.4	48 ± 1.2
R292E	4 ± 0.9	10 ± 0.5
R292Q	5 ± 1	17 ± 0.7
R292A	7 ± 0.4	23 ± 1.8
Δ271-294	0.4 ± 0.7	0.9 ± 0.1
Δ279-294	1 ± 0.6	5. ± 0.2
Δ287-294	7 ± 1.9	14 ± 1
Δ291-294	7 ± 1	15 ± 0.7
Δ294	20 ± 2.7	47 ± 2

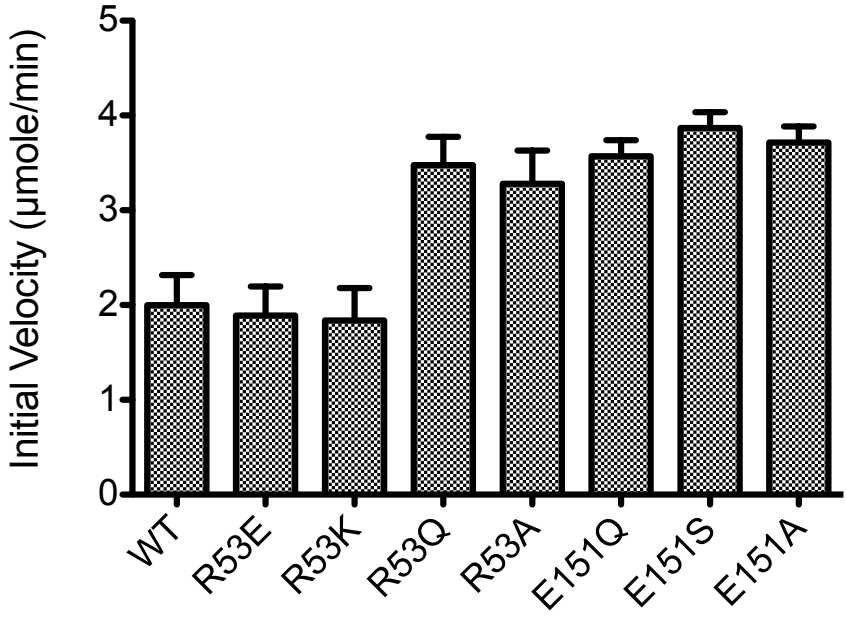

Figure 3.10 Glutaminase activity for PdxS R53 and E151 substitutions.

The C-terminal tail serves as a lid that covers helices α2a and α8' and the KGEPG loop, but does not directly contact the covalent intermediate. The tail is not fully ordered, but combination of densities from the six independent subunits in the crystallographic asymmetric unit permitted all but the last four amino acids to be built into electron density (Fig. 3.8). Tail residues Pro285, Glu286, and His287 contact Arg53 and the KGEPG loop. The C-terminal tail interacts with the PdxS core in a zippered network of hydrogen bonds alternating between side chain and backbone atoms. For example, the His287 side chain (tail) forms a hydrogen bond with the Gly150 carbonyl (core, KGEPG). The Gln290 side chain (tail) forms a hydrogen bond to the Glu112 backbone carbonyl (core) while the His115 side chain (core) forms a hydrogen bond to the Gly290 backbone amide. In all six monomers, density for the tail ends at Gln290 (Fig. 3.8). Interestingly, density for the tail ends near Arg137 (core) at precisely the binding site for phosphate in the R5P adduct at Lys149, for at Gln290 (Fig. 3.8). The Gln290 backbone carbonyl forms a hydrogen bond to Arg137 (core) at precisely the secondary phosphate site for the phosphate in the R5P adduct at Lys149 (Fig. 3.11), for phosphate in the PdxS free enzyme[48], and for PLP phosphate in the yeast synthase structure[50]. Thus the ordered C-terminal tail is incompatible with phosphate-containing ligands in this site. Interestingly, the Lys149 side chain is outside the active site pointed towards the secondary phosphate site, unlike its position in the PdxS/R5P/NH_3 structure.

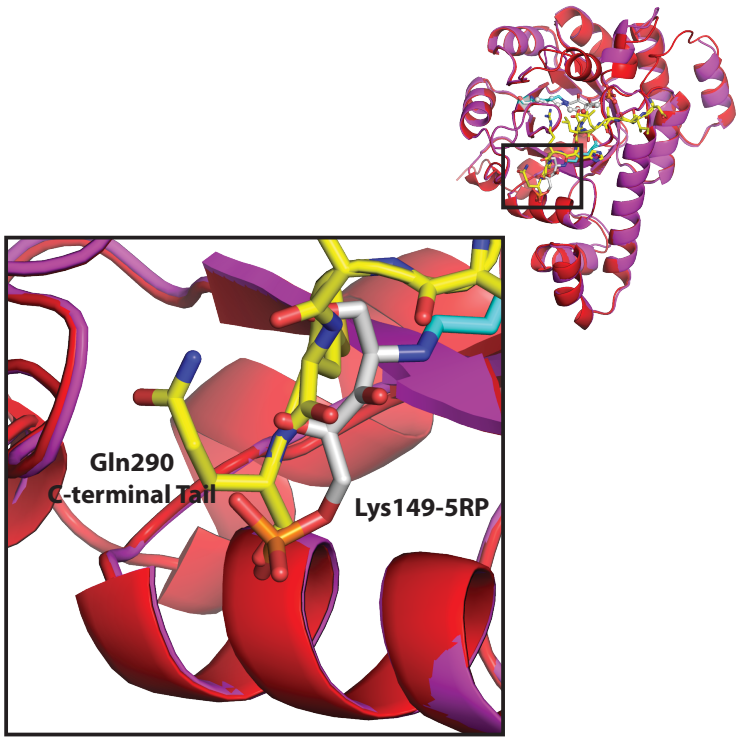

Figure 3.11 C-terminal tail overlaps secondary phosphate binding site. The last observable residue (Gln290) of the C-terminal tail (yellow sticks) in the structure of PLPS/H169N$_T$/Gln/R5P (red/gray sticks) binds to the same site as the second adduct phosphate (gray sticks) in the PdxS/R5P structure (magenta/cyan sticks).

The entire length of the C-terminal tail is essential to chromophore formation. I made several C-terminal truncations (PdxSΔ271-294, PdxSΔ279-294, PdxSΔ287-294, PdxSΔ291-294 and PdxSΔ294) to evaluate whether the entire tail is essential to catalysis (Table 3.7). As expected, the tail truncations had no effect on the PdxT glutaminase activity (Fig. 3.12). All truncated variants had decreased chromophore formation and PLP synthesis, with a greater effect on chromophore formation. The reduction in activity was correlated with the size of the truncation, but removal of even one amino acid (Δ294) reduced activity five fold for chromophore formation and two fold for PLP synthesis (Table 3.7). The four residues not observed in this structure were

Glu291-Arg292-Gly293-Trp294. Trp294 and Arg292 are the only conserved residues among these four. Substitutions at conserved Arg292 had a greater effect on both chromophore and PLP formation compared to substitutions at the non-conserved Glu291. Retaining the positive charge at position 293 (R292K) was least deleterious.

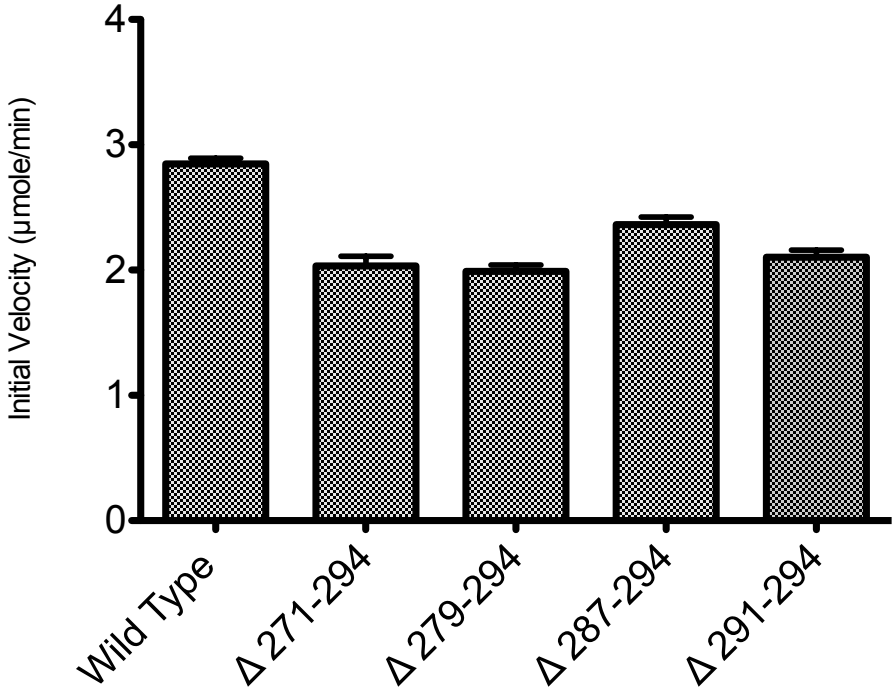

Figure 3.12 Glutaminase activity for tail truncation variants.

Discussion

Our studies present the first structure of intact PLPS with more than one substrate and an ordered C-terminal tail. Covalently trapping the amino ketone intermediate in PdxS and the γ-glutamyl thioester intermediate in PdxT was sufficient to promote a “closed” conformation of PdxS. The closed state results from multiple structural elements layered over the synthase active site protecting the R5P active site

by burying R5P in a solvent-inaccessible cavity within the core of PdxS. The structural elements responsible for this protection include helices α2a and α8', the KGEPG loop and the C-terminal tail. In addition to aiding in the closing of R5P active site, the C-terminal tail hydrogen bonds to core residues residing on the adjacent subunit (Fig. 3.13). Hydrogen bonds are formed between the carbonyl of Met275 (C-terminal tail) and the side chain of Arg60 (helix α2a in adjacent subunit), the carbonyl of Arg276 (C-terminal tail) and the amide nitrogen of Val58 (neighboring of helix α2a), and the carbonyl of Gly155 (KGEPG loop) and the side chain of Arg60. Cooperativity was not observed in the activity of PLPS but these interactions connect adjacent subunits around the structural elements that facilitate the closing of PdxS. Consistent with the lack of cooperativity, the orientation of each subunit relative to its neighbors is unchanged by active site closure. These movements taken together reveal the mechanism for creating a protective cavity where the conversion of the amino ketone intermediate to the chromophore intermediate can take place. Perturbations of specific residues forming the interactions necessary to create the solvent inaccessible R5P cavity significantly decrease the ability of PdxS to generate the chromophore, suspending the remaining steps of catalysis.

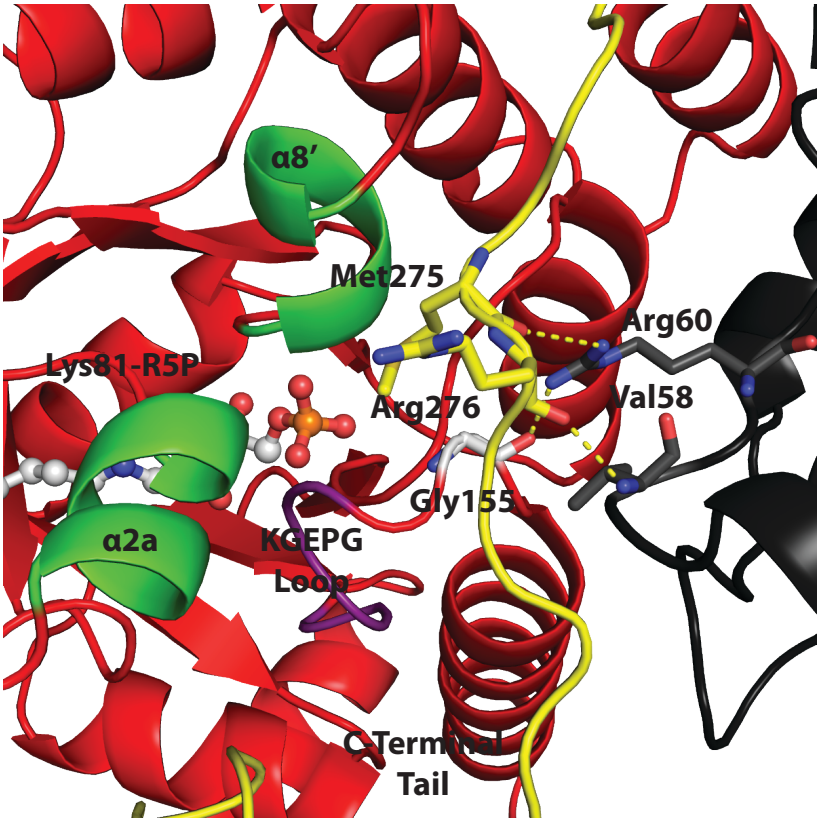

Figure 3.13 Contacts between adjacent subunits. Residues on the C-terminal tail (yellow) of the PdxS red subunit form hydrogen bonds with core residues on the adjacent gray subunit.

I propose a model for the dynamic role structure plays in the catalytic mechanism of PLPS. This model is supported by the structure and is consistent with my and others' biochemical data. The closed structure is a snapshot of PLPS in anticipation of converting the amino ketone intermediate to the chromophore intermediate. PdxS has a highly ordered catalytic mechanism in which structural changes ensure that each substrate is at the correct position at the correct step in catalysis. I propose that the closed state of PdxS is essential to the formation of the chromophore and is activated by the presence of covalent intermediates in both the glutaminase and synthase active sites. The solvent-inaccessible R5P active site allows for a safe incorporation of reactive

ammonia into the amino ketone intermediate. The effectiveness of the substrate cavity is dependent on tight regulation.

The first step in preparation for chromophore formation is the formation of the solvent-inaccessible cavity. Changes in proteolytic susceptibility and tryptophan fluorescence demonstrated that the C-terminal tail changes conformation in the presence of substrates[6]. The closed structure confirms that the C-terminal tail acts as a lid induced by both the γ-glutamyl thioester and amino ketone covalent intermediates. I propose that the structural movements observed among the *G. stearothermophilus* structures are dependent on both covalent adducts and that PdxS closure occurs before the ammonia channel from PdxT to PdxS opens. Structures of PLPS from *B. subtilis* and *T. maritima* each contain one covalent modification (either the γ-glutamyl thioester intermediate or the amino ketone intermediate) and either one alone was not sufficient to order the C-terminal tail of the synthase subunit. Consistent with this hypothesis, both of the synthase structures reported in Chapter 2 are in an open conformation (Fig. 3.14). This suggests that the simultaneous closing of PdxS and the ordering of the C-terminal tail are only induced in preparation for ammonia incorporation into the amino ketone intermediate.

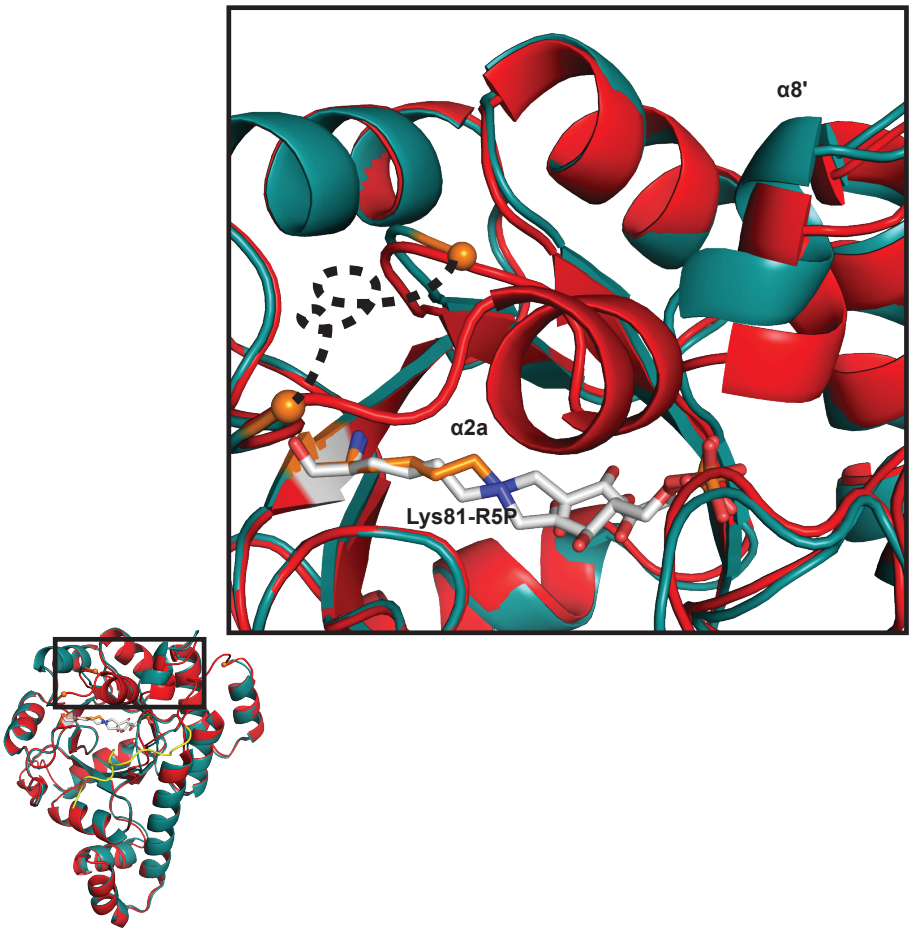

Figure 3.14 Comparison of PLPS/H169N$_T$/R5P/Gln and PdxS/R5P/NH$_3$. PLPS/H169N$_T$/R5P/Gln (red) is in a closed conformation in comparison to other *G. stearothermophilus* structures (PdxS/R5P/NH$_3$; teal).

To protect the labile ammonia, the timing of ammonia release into the R5P active site requires regulation. This regulation would prevent ammonia from entering into the cavity until the R5P active site is closed. One defining characteristic of GATs is the ammonia channel that transfers the ammonia generated in the glutaminase domain to the synthase domain[5]. The structure reported here supports the hypothesis that the R5P active site closes before the channel from PdxT to PdxS opens, due to a lack of an unobstructed tunnel between the two subunits. The proposed PdxS methionine-rich tunnel (residues 13,79,145 and 43) is closed in this structure with all residues in the

same positions as in previous structures of intact PLPS[9,49]. These observations support my hypothesis that the closed structure is a snapshot of PLPS before the channel between the two active sites opens.

In addition to sequestering ammonia generated by PdxT and ensuring its safe incorporation into the amino ketone, the cavity would also protect the intermediate during a proposed C-N bond shift[56]. It has been proposed that the amino ketone intermediate experiences a C-N bond shift that switches the Lys81 attachment from C1 to C5 upon chromophore formation[56,57]. Therefore, the solvent-inaccessible cavity serves dual purposes of protecting and incorporating ammonia and sequestering the intermediate during conversion from C1 attachment at Lys81 to C5 attachment.

PLPS differs from other GATs in the regulation of glutamine hydrolysis. The paradigm for GATs is that glutamine hydrolysis is prevented or diminished in the absence of the acceptor substrates, ensuring that the glutaminase and synthase active sites are coupled[1]. PLPS is the only known GAT in which the glutaminase activity does not depend on, nor is accelerated by, the synthase substrates[8]. In fact, glutamine hydrolysis is dependent only on the formation of the intact PLPS[8]. One explanation for the unique PLPS behavior is that unlike other GATs all three substrates (glutamine, R5P and G3P) are readily available. The estimated intracellular concentrations of the substrates in bacterial cells are: DHAP (the isomer of G3P, which can also be used in the place of G3P[40]) 0.37 mM[110], R5P 0.15 mM[111] and glutamine 3.8 mM[110]. The K_m values for the three substrates are drastically different (glutamine, R5P and G3P are 600 ± 70 μM, 10 ± 2 μM and 1600 ± 400 μM). The K_m for G3P is higher than the other two substrates suggesting that DHAP/G3P is the limiting substrate. I propose that once

the chromophore is formed, addition of G3P is solely based on the proper orientation with respect to the chromophore without the use of catalytic residues from the PdxS. R5P does not appear to be limiting, but the efficacy of chromophore occupancy when glutamine is the nitrogen source in comparison to ammonia adds a component of coupled activity[54]. The use of common metabolites as substrates to generate PLP, an essential co-factor, is the brilliance behind PLPS. Up to 1.5% of prokaryotic genes encode for PLP dependent enzymes, therefore, the demand for PLP as a cofactor is immense[25]. In combination with readily available substrates (glutamine, R5P and G3P) suggests that regulation of PLPS at the protein level is unnecessary and accounts for why the two active sites are uncoupled. *Corynebacterium glutamicum* ATCC 13032 contains a gene, *PdxR*, which encodes a regulatory protein that controls the biosynthesis of PLP[112]. Therefore regulation of PLPS may be facilitated through another protein and not by the structure of PLPS.

Chapter 4

CTPS: Probing the binding site of the allosteric effector GTP

Summary

Cytidine triphosphate synthetase (CTPS) is the sole biosynthetic route to CTP in prokaryotes and eukaryotes, and occurs through activated amination of UTP. The reaction is dependent on ammonia (obtained through glutamine hydrolysis), ATP and Mg^{+2}. In addition to its substrates, CTPS activity is tightly regulated by the concentrations of CTP and GTP. CTP is an inhibitor and GTP is an allosteric activator. The activity of CTPS from the bacterium *Aquifex aeolicus* (Aa) is enhanced 3-4 fold in the presence of GTP with a K_{act} value of 1 μM[77]. In comparison to CTPS from other organisms, this is the lowest reported K_{act}. The current hypothesis is that GTP enhances the ability of CTPS to form the glutamyl thioester intermediate by facilitating a large conformational change that enhances glutaminase activity. Many biochemical methods have been used to probe the mechanism of GTP activation, resulting in the current hypothesis but no structural data are available to address the mechanism. I attempt to directly test the current hypothesis of GTP activation through structural biology. Using a glutamine analog (6-diazo-5-oxo-L-norleucine, DON) to mimic the glutamyl thioester intermediate, I co-crystallized Aa CTPS with UTP and GTP. In addition to X-ray crystallography, negative stain electron microscopy and thermal stability binding experiments were used to monitor structural changes brought about by GTP binding.

Introduction

Cytosine triphosphate synthetase (CTPS) is responsible for the conversion of UTP to CTP. In *A. aeolicus,* CTPS consists of a single polypeptide that includes an N-terminal synthetase domain (266aa), an inter domain linker (18aa) and a C-terminal glutaminase domain (244aa)[77]. CTPS oligomerizes to form a homo-tetramer with D_2 symmetry to form an overall cross shape (Figure 4.1)[87]. The glutaminase domain of CTPS is classified as a Triad glutamine amidotransferase (GAT) that uses a Cys-His-Glu catalytic triad to generate ammonia through glutamine hydrolysis. The ammonia is channeled to the synthetase domain where UTP is activated through phosphorylation by ATP[7]. Nucleophilic attack by ammonia displaces phosphate converting UTP to CTP[7]. Glutaminase and synthetase activities are tightly coupled, and the glutaminase activity is dependent on the presence of the acceptor substrate UTP[77]. Nucleotide levels tightly regulate CTP formation. In addition to binding the substrates UTP and ATP, the product CTP is a potent inhibitor and GTP is an allosteric activator[67-70].

The mechanism of GTP activation has remained a mystery. Structures of CTPS from several biological sources have been determined with various combinations of substrates[80,87,113,114]. In all of the structures the glutaminase active site is open to solvent and remote from the synthetase active site. It is unknown how CTPS sequesters labile ammonia and channels it to the acceptor substrate. Kinetics, thiol reactivity experiments, mutagenesis and activity assays support a hypothesis for GTP activation in which GTP facilitates a conformational change that enhances the ability of CTPS to form the glutamyl thioester intermediate and also an ammonia channel between the glutaminase and synthetase active sites[71,78,115,116]. Using the knowledge gained from

biochemical assays I attempted to answer two important questions: where is the GTP binding site and how is the ammonia channel formed?

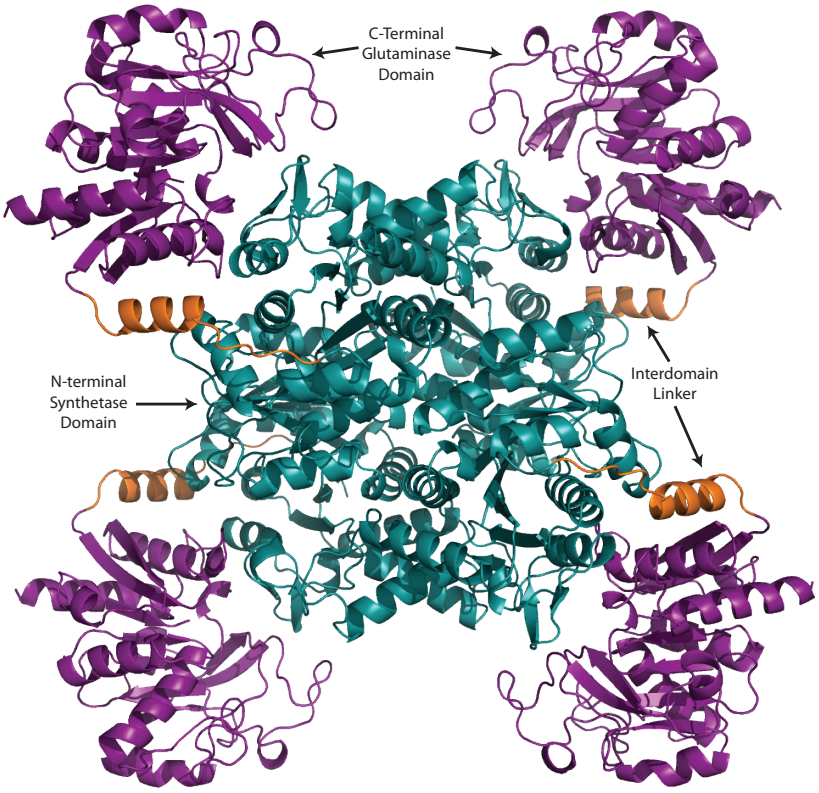

Figure 4.1 CTPS homo-tetramer. Each monomer consists of two domains, a glutaminase domain (purple) and a synthetase domain (teal). The domains are separated by an interdomain linker (orange)[77].

Like most amidotransferases, CTPS can use either glutamine or ammonia as a nitrogen source. GTP increases the rate of CTP synthesis when glutamine is the nitrogen source while having no effect when NH_3 is the nitrogen source suggesting that GTP has no effect on steps subsequent to glutamine hydrolysis[71]. The rate-limiting step for glutamine hydrolysis is the formation of the glutamyl thioester intermediate. GTP both decreases the K_m for glutamine and increases the k_{cat} for glutaminase activity[71].

Biochemical experiments with glutamine analog inhibitors revealed that GTP activation was abolished when the glutamylation step was interfered with, that GTP increases the rate of modification of the nucleophilic cysteine 8-fold, and that GTP decreases the K_i 10-fold[71,78,115]. CTPS activation does not consume GTP[76]. Tests with analogs demonstrated that the sugar, base and triphosphates are all required for activation and binding [117]. GTP specificity was demonstrated as a requirement for the 2-amino substituent on the guanine base[68,117].

Two regions of CTPS have been implicated in GTP activation and proposed as binding sites (Fig. 4.2). Sequence alignments identified a region on the glutaminase domain (residues 438-444) where substitutions decreased GTP activation[87,118,119]. Scanning alanine mutagenesis identified a region on the synthetase domain (residues 111-130) where substitutions impaired GTP activation and glutamine-dependent CTP synthesis[87,116]. The distance between the two sites is 25 Å within one subunit and 15 Å between adjacent subunits (Fig. 4.2)[87]. If GTP bridges the sites, a large conformational change would be needed to bring the sites in proximity.

Additionally, temperature factor analysis of crystal structures revealed that the domain interface is flexible, suggesting that the glutaminase domain may move closer to the synthetase domain during catalysis[87]. A series of CTPS structures from *Thermus thermophilus* revealed a hinge motion of 25° between the domains in nonphysiological conditions and a minimum distance between the two active sites of 7 Å[87]. Other evidence of large-scale flexibility includes an ATP/UTP-induced change in the tetramer hydrodynamic radius observed by dynamic light scattering[87]. The best example of changes to the overall shape of the homo-tetramer induced by substrate/product

binding is that of Aa CTPS. Crystal structures of product-inhibited and substrate bound CTPS differ by a 3.6° rotation between the synthetase domains, supporting the ability of CTPS to rearrange the interfaces between adjacent subunits[77].

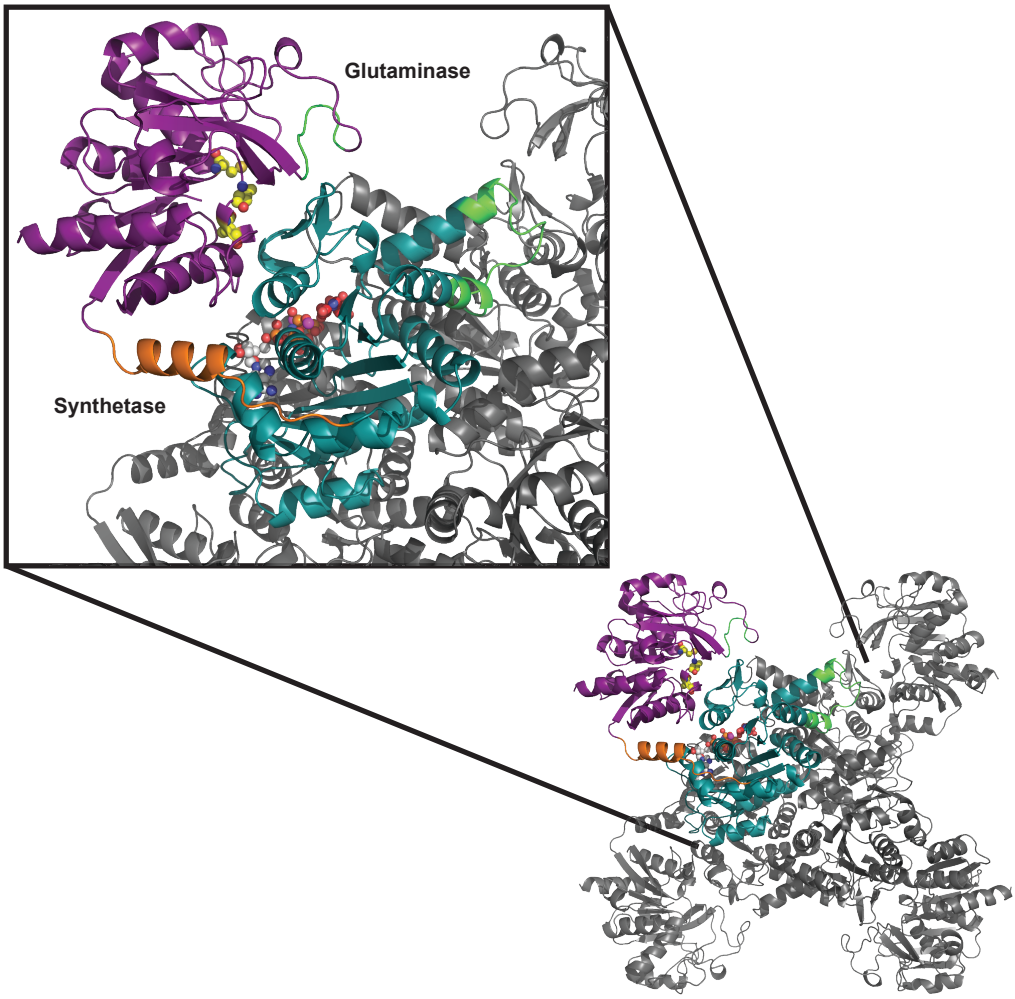

Figure 4.2: Proposed GTP binding sites. Two regions have been proposed as potential GTP binding sites (green), one on the glutaminase domain (purple) and one on the synthetase domain (teal). These regions are located 15-25 Å apart. Glutaminase catalytic triad; yellow spheres, UTP binding site; gray spheres.

Structural studies of CTPS treated with DON suggest that the glutamyl thioester intermediate in the presence of GTP induces conformational changes within CTPS, as the cysteine thiol groups of CTPS are less reactive when CTPS is treated with DON

verses glutamine[115]. All GATs must sequester labile ammonia and channel it to the synthetase active site. An ammonia channel within CTPS has not been visualized[77,87]. CTP is produced in a one to one ratio with UTP, ATP and glutamine/NH_3 consumption[76]. Glutaminase activity is inhibited by ammonia supporting one pathway/site for ammonia[76]. The conformational change induced by the formation of the glutamyl-intermediate and/or GTP binding may also form the ammonia channel.

The objective was to use structural and binding experiments to elucidate the GTP binding site of CTPS from the bacterium *Aquifex aeolicus*. CTPS was co-crystallized in the presence of DON in an attempt to observe the conformation of CTPS as the glutamyl intermediate and to provoke the binding of GTP. The resulting structure was not significantly different than other structures, no ammonia channel formed, and a novel nucleotide-binding site was not identified. Mutagenesis was used in an attempt to escape the predominant crystal form. Unfortunately the familiar CTPS tetramer and crystal form occurred with the variant. Binding experiments were conducted on an excised glutaminase domain and the full length Aa CTPS in order to distinguish whether GTP binds solely to the glutaminase domain or to both domains. GTP had no stabilizing effect on either protein. A construct of the excised synthetase domain was unsuccessful due to folding and solubility problems.

Experimental Procedures

Cloning of A. aeolicus CTPS

The plasmid pET28a-CTPS[77] was used for all mutagenesis and sub-cloning. Substitutions were generated by site directed mutagenesis (QuikChange by Strategene).

The glutaminase domain of CTPS was generated by sub-cloning a construct encoding amino acids 273-531. Primers are listed in Table 4.1/4.2.

Table 4:1 Primers used for SDM.

Primers for SDM				
Plasmid Name	**Mutation**	**Expression Vector**	**Direction**	**Primer**
pCTPSH502N	H502N	pET28a	Forward	5'-CTTGAACTCGGGGTTGAACTGACATCCCA-3'
pCTPSXtal_1	N395S/D404H	pET28a	Forward	5'-GAACGTTCTCGGATTTAGTAGCGCAAACTCAACGGA-3'
			Forward	5'-GGAGTTCGACCCCCATACACCGTTCCC-3'
pCTPSXtal_2	R34E/R268E/K277E/ N395D/D404H	pET28a	Forward	5'-CTCGAAGAAATGGGCTACGAGGTTACCCTCCAGAAGCT-3'
			Forward	5'-AAGACTGAACCTTGAACACGAGGAAGTTAACCTCGGGAAG-3'
			Forward	5'-ACCTCGGGAAGTGGAAGGAGATAGTAAACGTCCTA-3'
			Forward	5'-CGCAAGGAACGTTCTCGGATTTAGTGACGCAAACTCAAC-3'
			Forward	5'-GGAGTTCGACCCCCATACACCGTTCCC-3'

Table 4:2 Primers used to generate excised glutaminase domain.

Primers for Sub-Cloning					
Plasmid Name	**Start**	**End**	**Expression Vector**	**Direction**	**Primer**
pCTPS_Gln	273	531	pET28a	Forward	5'-GCGCCATGGGGAAGTGGAAGAAGATAG- 3'
				Reverse	5'-GCGAAGCTTCTACGTAACTTTCTCTT-3'

Expression and Purification of CTPS.

The growth conditions for each protein and protocols for purification are listed in Table 4.3. Cells of *E. coli* strain BL21 pRARE(DE3) were transformed with the appropriate expression plasmid, grown at either 25°C or 37°C in Luria-Bertani (LB) or Terrific Broth (TB) medium containing 50 mg/mL kanamycin and spectinomycin for approximately 20 hr without induction or until OD_{600} reached 1. Once the OD_{600} reached 1 the temperature was reduced to 20°C for 1 hr, expression was induced with 100 μM IPTG, and cultures were incubated 12-16 hr. Cells from a 1 L culture were harvested by centrifugation, re-suspended in 40 mL lysis buffer (20 mM MOPS pH 7.5, 50 mM NaCl, 2 mM $MgCl_2$), lysed by sonication, and centrifuged at 18,000 x g. CTPS from the hyperthermophile *A. aeolicus* was purified from *E. coli* proteins by heat treatment. The supernatant was heated 10 min at 80°C, centrifuged 20 min at 18,000 x g. The

supernatant was re-heated and centrifuged in the same manner. The supernatant was incubated 2 hr with 90U/mL of Benzoase Nuclease (Sigma-Aldrich) at 37°C. CTPS was then purified on an S200 column (HiLoad^{TM} 16/60 Superdex^{TM} S-200 HR, GE Healthcare) using 20 mM Tris pH 8.5, 50 mM NaCl, 5% glycerol. The excised glutaminase domain was not stable to heat purification. After lysis and centrifugation, the supernatant from cells bearing pCTPS_Gln was filtered and loaded onto an ion exchange column (HiTrap^{TM} FF, GE Healthcare). Bound protein was eluted with a linear gradient of 0.05-1 M NaCl in lysis buffer. Pooled fractions containing the glutaminase domain were further purified on the S200 column using 20 mM Tris pH 7.9, 500 mM NaCl, 2 mM $MgCl_2$, 5% glycerol. Gel filtration fractions were monitored by A_{280}, A_{260} and SDS-PAGE (Fig. 4.3). Purified proteins were concentrated to ~10 mg/mL and stored at -80°C.

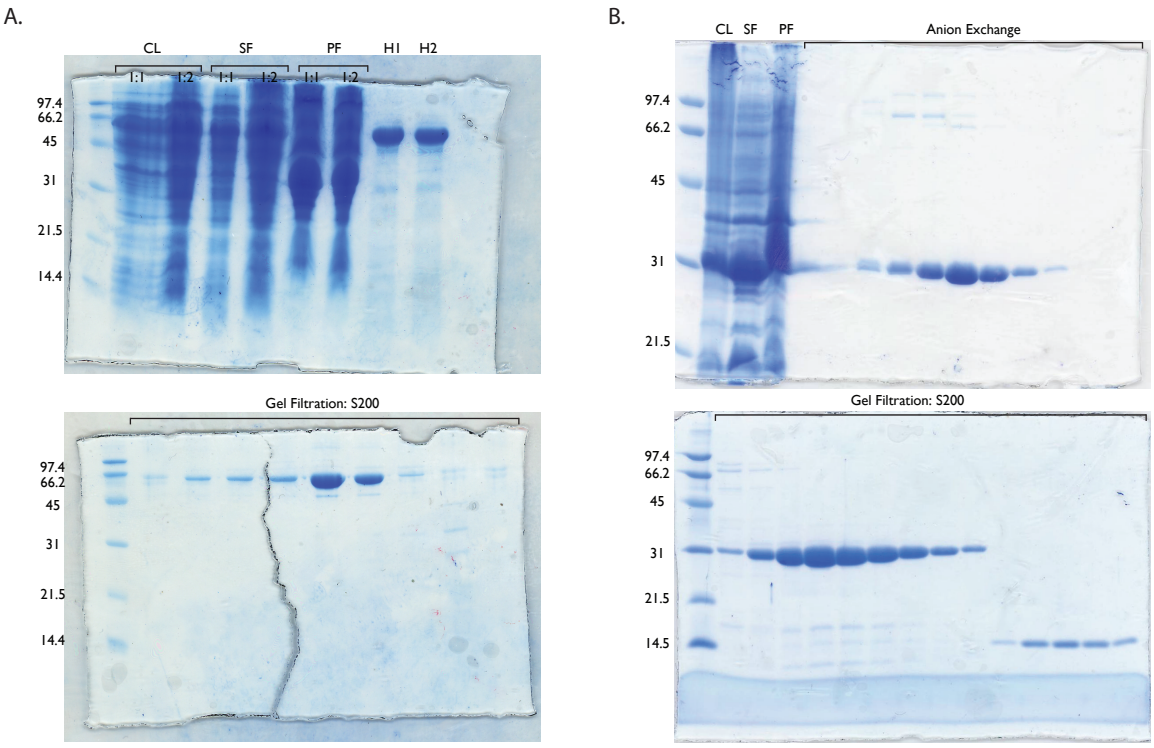

Figure 4.3 SDS PAGE of Full length CTPS and the excised glutaminase domain. A. Each full-length monomer of CTPS has a molecular weight of 60.3 kDa. B. The excised glutaminase domain has a molecular weight of 29.9 KDa. CL: crude lysate, SF: Soluble fraction, PF: pellet fraction, H1: Post heat treatment 1, H2: Post heat treatment 2.

Table 4:3 Growth specifics for each construct.

Plasmid	Media	Purification
pCTPS	LB	Heat/S200
pCTPSH502N	LB	Heat/S200
pCTPSXtal_1	LB	Heat/S200
pCTPSXtal_2	TB	Heat/S200
pCTPS_Gln	TB	Ion Exchange/S200

DON inactivation

Inactivation reactions were carried out at 75°C in a reaction mix containing 20 μM CTPS, 50 mM MOPS pH 7.9, 20 mM $MgCl_2$, 5 mM KCl, 5 mM ATP, 0.5 mM UTP, 5 mM GTP, 50 mM glutamine and 0-250 μM DON. DON inactivation was monitored by assaying residual glutaminase activity using a coupled reaction with glutamate dehydrogenase (GDH)[8]. Aliquots (40 μL) were removed at 5-20 min and quenched with 10 μL 200 mM ethylenediaminetetraacetic acid (EDTA) to remove all nucleotides from the enzyme. GDH reactions were carried out at 37°C in a total reaction volume of 200 μL containing 40 μL of the quenched DON reaction, 100 mM Tris-HCl pH 8.5, 50 mM KCl, 0.375 mM 3-acetylpyridine adenine dinucleotide ($APAD^+$) and 1.8 μM GDH (Sigma). Glutamate formation was monitored by GDH reduction of $APAD^+$ to APADH detected at 363 nm using a SpectraMax M5 Multi-Mode Microplate Reader (Molecular Devices).

Crystallization

Wild type CTPS/DON/GTP/UTP was crystallized at 4°C via hanging drop vapor diffusion using 1 μL protein solution (7 mg/mL CTPS, 20 mM Tris-HCl pH 8.5, 50 mM NaCl, 5% (v/v) glycerol, 20 mM GTP, 5 mM UTP and 360 μM DON) and 1 μL reservoir solution (31% (w/v) PEG 3350, 250 mM Na citrate). CTPS was pre-incubated with DON before

the addition of the other substrates. Crystals appeared within 2 days, grew over 14 days, and were cryo-protected with 20% ethylene glycol in reservoir solutions and flash-cooled in liquid nitrogen.

CTPS N395S/D404H was crystallized at 20°C via hanging drop vapor diffusion using 1 µL protein solution (6 mg/mL CTPS, 20 mM Tris-HCl pH 8.5, 50 mM NaCl, 5% glycerol, 20 mM GTP, 5 mM UTP and 200 µM DON) and 1 µL reservoir solution (1.55 M Na citrate). CTPS was pre-incubated with DON before the addition of the other substrates. Crystals appeared within 2 days, grew over 14 days, and were cryo-protected with 15% ethylene glycol in reservoir solutions and flash-cooled in liquid nitrogen.

Wild type CTPS/DON/GTP was crystallized at 4°C via hanging drop vapor diffusion using 1 µL protein solution (7 mg/mL CTPS, 20 mM Tris-HCl pH 8.5, 50 mM NaCl, 5% (v/v) glycerol, 20 mM GTP and 360 µM DON) and 1 µL reservoir solution (2.1 M DL-Malic acid pH 7.0). CTPS was pre-incubated with DON before the addition of GTP. Crystals appeared within 2 days, grew over 14 days, and were cryo-protected with 15% (v/v) ethylene glycol in reservoir solutions and flash-cooled in liquid nitrogen.

X-ray Data Collection and Processing:

Data were collected at the Advance Photon Source (APS) at the GM/CA facility. Data were processed with MOSFLM[120] and HKL2000 (Table 4.4/4.5)[91]. Data were scaled and merged with SCALA[121] in the CCP4 suite[95]. Initial phases for each structure were determined by molecular replacement using the program phaser[93]. The structure of CTPS/UTP/ANP[77] was used to solve both the wild type structures (CTPS/UTP/GTP/DON and CTPS/GTP/DON) while, the structure of CTPS/CTP/ADP[77] was used to solve the CTPS/N395S/D404H/GTP/UTP/DON structure. Iterative model

building was done in COOT[94] and refinement was carried out with REFMAC[95]. Link records for the covalent modification of Cys376 with DON were generated using the coordinates for CYD from the structure of the human CTPS 2 glutaminase domain in complex with DON (PDB 2V4U). The library file for CYD was generated using PRODRG[99]. The final model was validated with MolProbity (Table 4.5 and Fig. 4.4)[101].

Table 4:4 Scaling statistics for CTPS/DON/UTP/GTP and CTPS N395S/D404H/DON/UTP/GTP.

CTPS/DON/UTP/GTP			
	Overall	**InnerShell**	**OuterShell**
Low resolution limit	59.91	59.91	2.00
High resoultion limit	1.90	6.01	1.90
R_{merge}	0.055	0.031	0.609
Rmerg in top intensity bin	0.039		
R_{meas}	0.06	0.034	0.757
R_{pim}	0.023	0.013	0.431
Total number of observations	352269	12803	18299
Total number of unique	56162	1934	5940
Mean ((I)/sd(I))	16	35.6	1.9
Completeness	92.6	94.5	68.2
Multiplicity	6.3	6.6	3.1
CTPS/N395S/D404H/DON/UTP/GTP			
	Overall	**InnerShell**	**OuterShell**
Low resolution limit	59.45	59.45	3.16
High resoultion limit	3.00	9.49	3.00
R_{merge}	0.217	0.144	0.453
Rmerg in top intensity bin	0.18		
R_{meas}	0.262	0.175	0.545
R_{pim}	0.144	0.098	0.299
Total number of observations	136049	4244	19857
Total number of unique	46521	1425	6948
Mean ((I)/sd(I))	3.8	6.4	1.7
Completeness	87.8	82	90.2
Multiplicity	2.9	3	2.9

Table 4:5 Crystallographic data and refinements statistics for CTPS/DON/UTP/GTP, CTPS N395SD404H/DON/UTP/GTP and CTPS/DON/GTP.

	CTPS/DON/UTP/GTP	CTPS N395S/D404H/DON/UTP /GTP	CTPS/DON/GTP
Diffraction data			
X-ray Source	APS 23ID-D	APS 23ID-B	APS 23ID-D
wavelength	1.033	1.033	1.033
space group	*I*222	$P2_1$	*I*222
unit cell parameters (Å)	89.3, 119.8, 143.2	105.1, 117.0, 111.2	89.6, 119.5, 142.6
α, β, γ (°)	90, 90, 90	90, 100, 90	90, 90, 90
asymmetric unit	1	4	1
resolution limit (Å)	1.9 (2.0-1.9)	3.0 (3.16-3.00)	2.48 (2.54-2.48)
unique reflections	53182	46521	27326
avg. I/σ_I	16 (1.9)	3.8 (1.7)	25.5 (3.7)
avg. redundancy	6.3 (3.1)	2.9 (2.9)	7.4(7.4)
completeness (%)	92.6 (68.2)	90.2 (87.8)	99.7 (100)
R_{sym}	0.06 (0.61)	0.22 (0.45)	0.06 (0.60)
Refinement			
data range (Å)	59.9-1.9	59.5-3.0	50.0-2.48
Reflections	53265	44005	25852
R/R_{free} (%)	21.2/24.6	28.8/36.9	22.4/29.1
RMS deviations			
bonds lengths (Å)	0.006	0.014	0.014
bond angles (deg)	1.050	1.663	1.840
average B factors (Å^2)			
protein	42.8	44	N/A
water	54.1	N/A	N/A
ligands	50.5	N/A	N/A
Ramachandran			
Favored (%)	97.9	N/A	N/A
Allowed(%)	1.5	N/A	N/A
Outlier (%)	0.6	N/A	N/A
Number of Atoms			
Protein	4221	16736	N/A
Water	224	N/A	N/A
Ligands	58	N/A	N/A

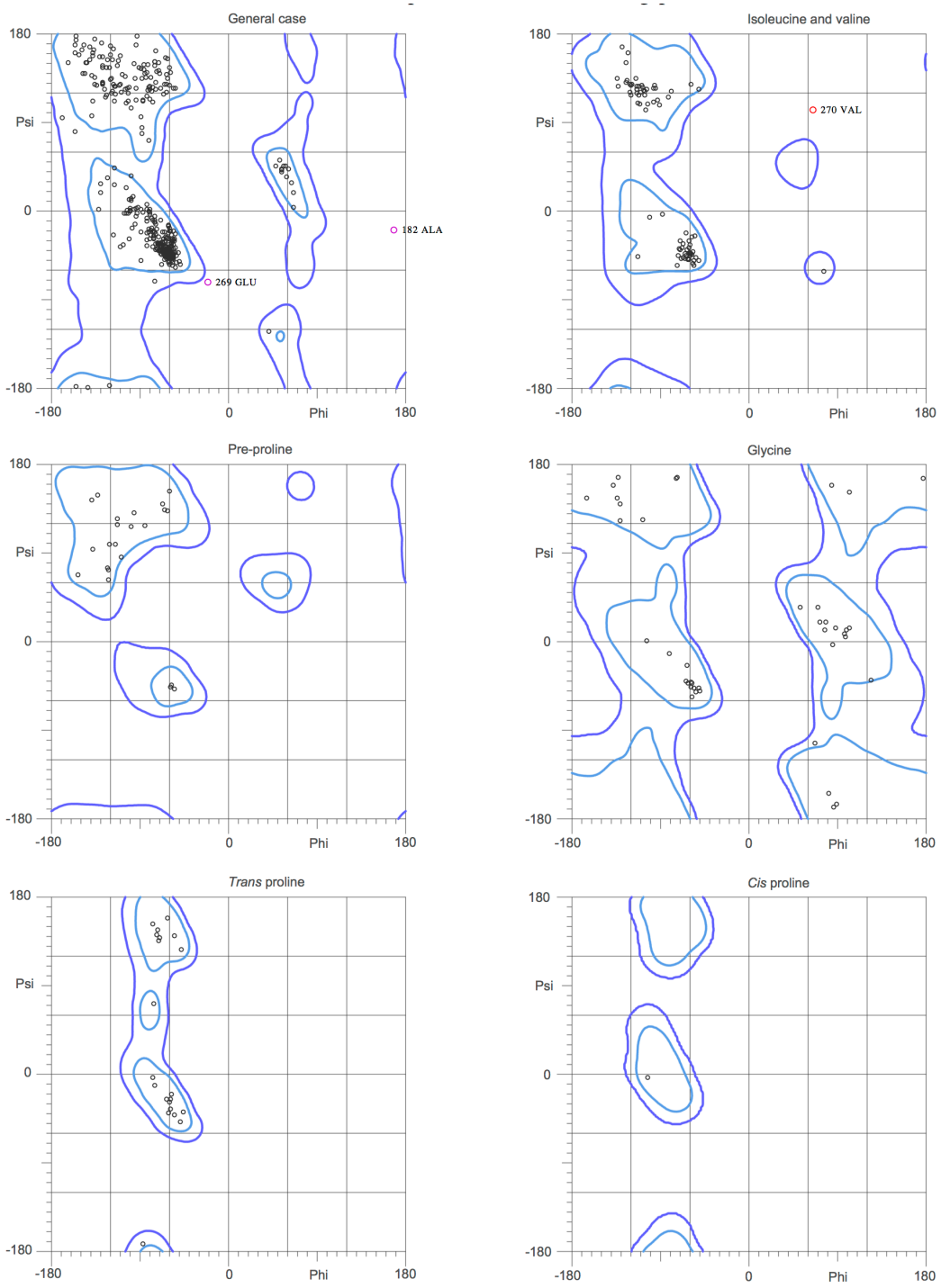

Figure 4.4 Ramachandran plot for CTPS/DON/UTP/GTP. Ramachandran plots for CTPS/DON/UTP/GTP indicate that 97.9% of all residues were in favored regions and 99.4% of all residues were in allowed regions. Plots were generated using Molprobity[101].

Electron Microscopy

Purified Aa CTPS (5 µL of 2 mg/mL) was incubated at 75°C for 5 min in 15 µL of activity buffer (50 mM Tris 8.5, 10 mM $MgCl_2$, 1 mM UTP, 1 mM ATP, ± 0.2 mM GTP, ± 10 mM Gln, ± 0.4 mM DON). Based on test images the sample was diluted to a protein concentration of 0.03 mg/mL, applied to a carbon-coated grid, and stained with 0.75% uranyl formate using standard protocols[122]. A Morgagni 286(D) transmission electron microscope equipped with a mounted Orius SC200W CCD camera was used for imaging.

Stability Experiments

The stability of full length CTPS or the excised glutaminase domain was assayed by fluorescence-based thermal shift using a ThermoFluor® 384 system. Denaturation was carried out in a total volume of 7 µL containing 5 µM protein in storage buffer (gel filtration buffer for either the full-length CTPS or the glutaminase domain), 0.2 mM 8-anilino-1-naphthalenesulfonic acid ammonium salt (ANS; Sigma-Aldrich) and 2 µL 100% silicone oil. ANS fluorescence was measured in 1°C increments from 37°C-95°C (30 sec incubation at the test temperature followed by 30 sec incubation at 37°C). In order for the full length CTPS to melt at a temperature within the range of the instrument, the test solution contained 1.0 M guanidinium chloride. Substrate effects on melting temperature were determined with 2.5 mM glutamine, 30 µM GTP, and 2.5 mM UTP.

Results

CTPS with DON modified nucleophilic cysteine.

I determined the structure of CTPS modified with DON and co-crystallized with UTP and GTP in an attempt to elucidate the GTP binding site. The concentration of DON to ensure 100% occupancy was assayed before co-crystallization (Fig 4.5), and a DON concentration twice the CTPS concentration was used for crystallization. The homotetramer is similar in overall structure to the free enzyme and nucleotide complexes of Aa CTPS[77]. Crystals were isomorphous with the crystals of Aa CTPS nucleotide complexes (*I*222) with one monomer in the asymmetric unit. There is clear evidence of covalent modification of the nucleophilic Cys376 with DON (Fig. 4.6B). DON forms many interactions with the protein, including hydrogen bond of the C2 ketone with the amide nitrogen of Gly349, the Cα amino group with the carbonyl of Gly349 and the side chain of Glu400, and the Cα carboxylate with the side chain of Gln380 and the amide nitrogens of Tyr458 and Arg457 (Fig. 4.6A).

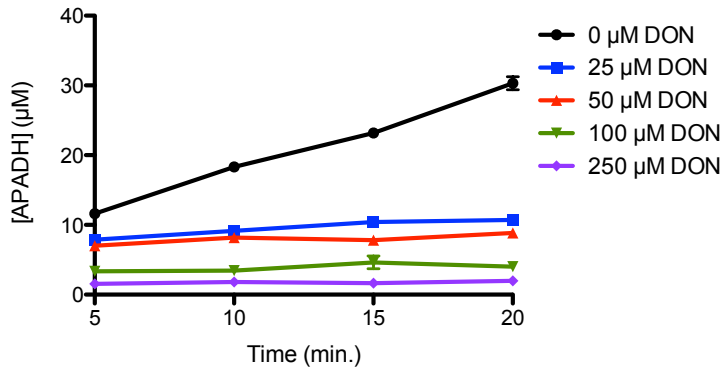

Figure 4.5 DON inactivation of Aa CTPS glutaminase. Glutaminase activity was assayed in the presence of varying concentrations of DON in order to determine the concentration (20 μM CTPS) needed to modify 100% of the glutaminase active sites in the crystal.

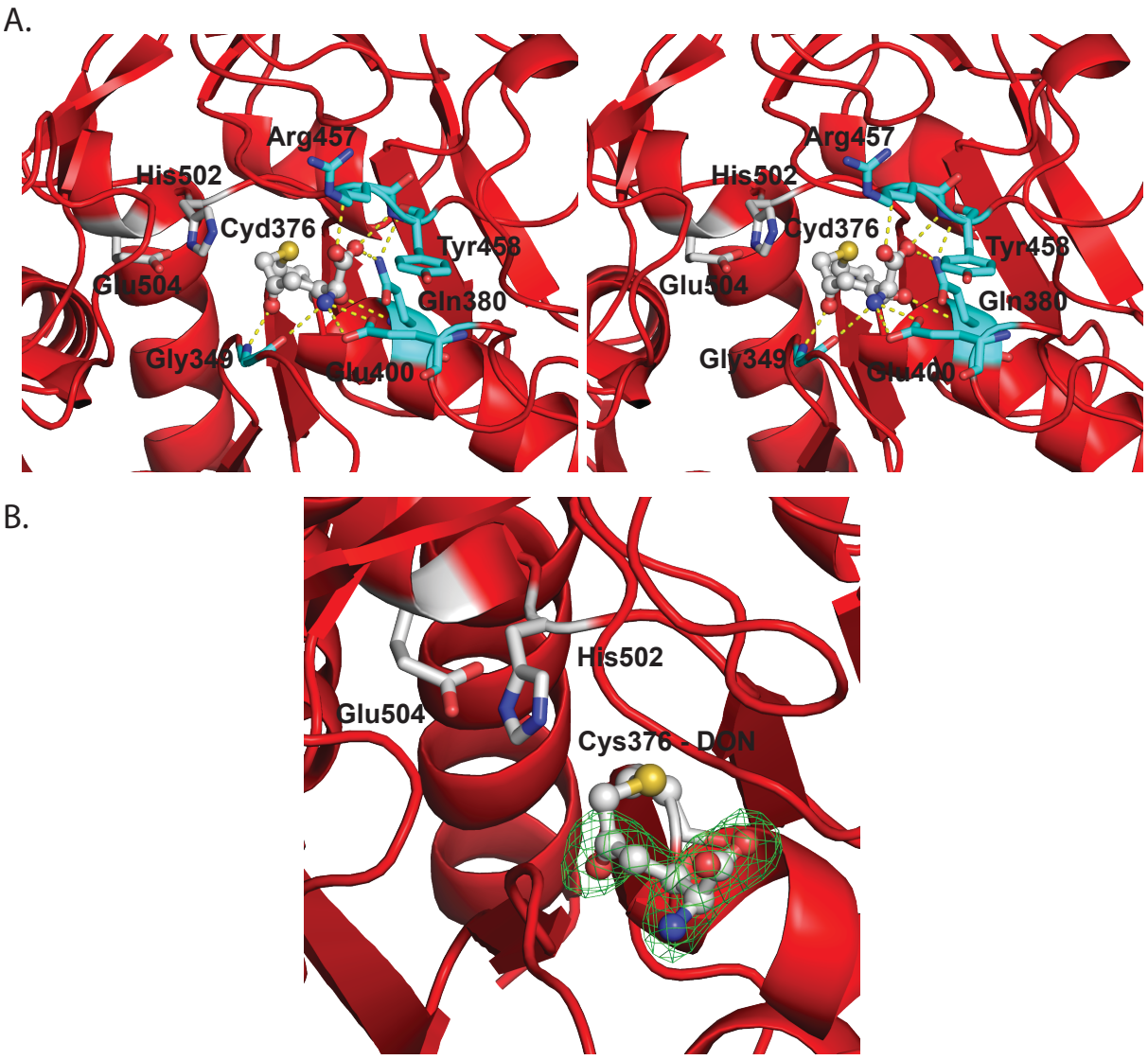

Figure 4.6 Nucleophilic Cys376 modified with DON. A. DON (gray sticks) interacts with many conserved residues (cyan sticks). B. Strong density (green; $F_o - F_c$, omit density contoured at 3 σ,) is present for the covalent modification of Cys376 (gray sticks) of the catalytic triad (gray sticks).

In the synthetase domain the known UTP site has strong density for triphosphate, but no density for ribose or uracil (Fig. 4.7A). The triphosphate group forms hydrogen bonds with the side chains of Lys186, Thr187, Gln191 and Lys222 and the amide nitrogen of Thr187 of the adjacent monomer (Fig. 4.7C). Intriguingly, UTP also binds to the ATP site (Fig. 4.7B/4.8). The triphosphate group forms hydrogen bonds with the

side chains of Lys17, Lys 301 and Ser14 and the amide nitrogens of Gly18, Lys17, Gly 16 and Leu15. The 5-oxolane on the sugar forms a hydrogen bond to the side chain of Arg 210. The uracil base forms hydrogen bonds with the carbonyl of Pro238 and the amide nitrogen of Leu240. Many of these residues interact with ATP in the nucleotide complexes of Aa CTPS[77].

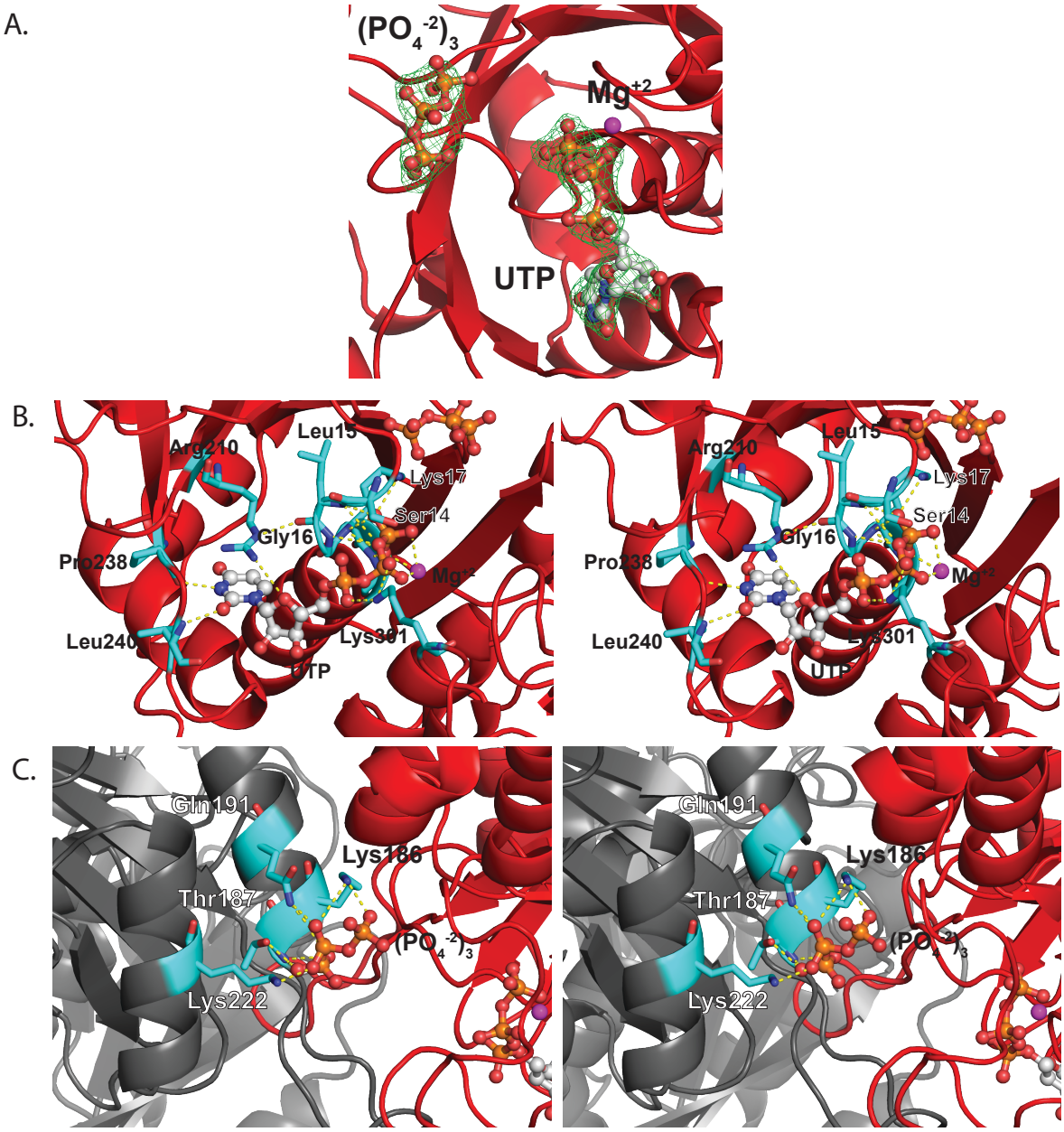

Figure 4.7 Nucleotide binding. A. Triphosphate and UTP density (green; F_o- F_c; omit density contoured at 3 σ). The triphosphate is in the UTP site, and UTP (gray sticks) is in the ATP site. B. UTP interactions (stereo). C. Triphosphate interactions (stereo).

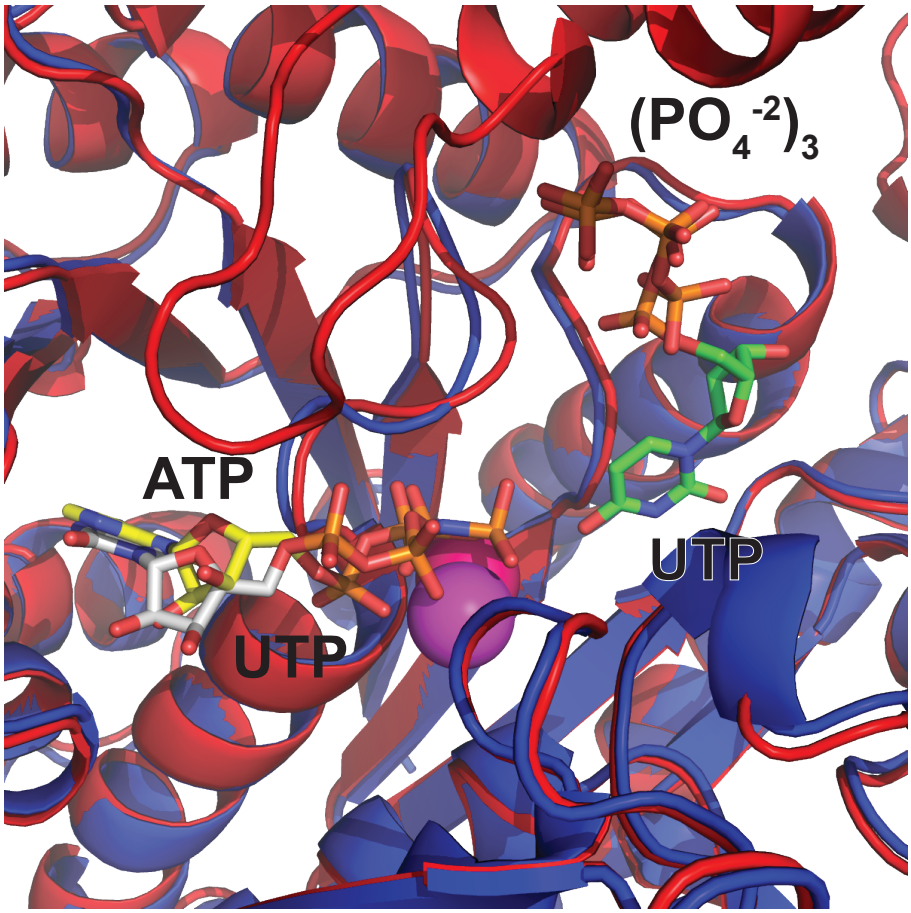

Figure 4.8 Superposition of CTPS/DON/UTP/GTP (red) with the CTPS/UTP/ANP structure (blue) show that UTP binds exactly where ANP (yellow) is bound and the triphosphate group binds exactly where the triphosphate group of UTP (green) binds[77].

Disrupting the *I*222 crystal contacts.

All structures of *A. aeolicus* CTPS are from crystals of the same space group *I*222 (Fig. 4.9A). If the hypothesis is correct that GTP induces a large CTPS conformational change, then the conformation favored by crystal packing may prevent observation of other CTPS conformations. To overcome this, site directed mutagenesis was conducted on non-conserved residues participating in the sole tetramer-tetramer

crystal contact in order to prevent this interaction. These residues reside on a non-conserved loop in the glutaminase domain (residues 392-407) that is in the same orientation in all known Aa CTPS structures. I attempted to disrupt a salt bridge between Asp404 and a Lys277 and a hydrogen bond between Asn395 and the backbone carbonyl of Glu29 (Fig. 4.9B). Asn395 was substituted with serine and Asp404 with histidine. Diffraction quality crystals were obtained with this variant and a structure was determined at 3 Å in a new space group $P2_1$. Unfortunately, after molecular replacement and comparison with previous Aa CTPS structures, the overall organization was exactly the same and GTP binding was not observed. Other attempts to crystallize Aa CTPS with GTP included inactivating the glutaminase domain through substitution of the catalytic histidine with asparagine to prevent the release of glutamate in order to trap the natural glutamyl thioester. Diffraction quality crystals were obtained and structures were determined but none contained either GTP or the thioester intermediate in the glutaminase active site. A second variant of Aa CTPS was generated with more substitutions at the crystal contact either on the loop previously identified or in the synthetase domain on the opposite side of the crystal contact (R34E, R268E, K277E, N395D and D404H) (Fig. 4.9C). Crystals obtained with this variant were not of diffraction quality.

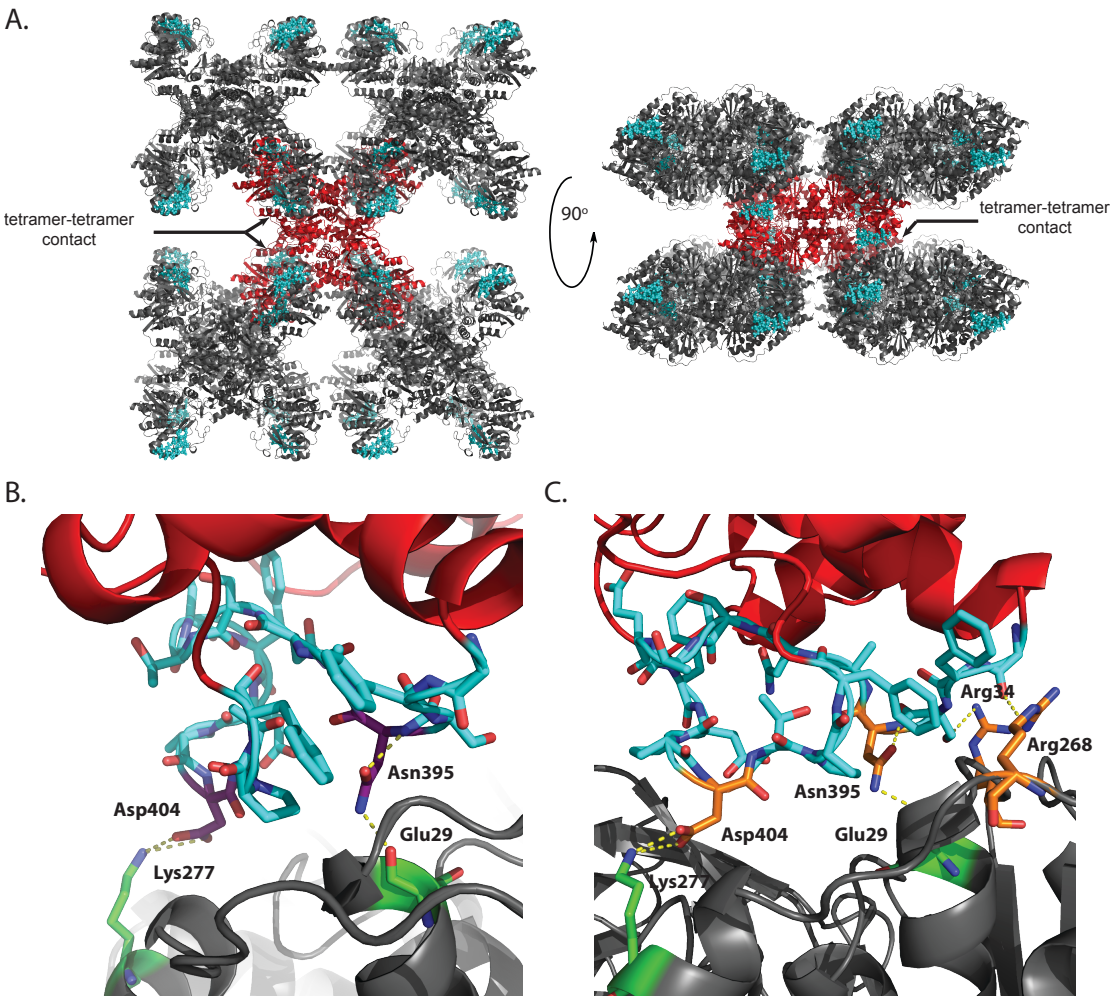

Figure 4.9 Disrupting the crystal contacts of Aa CTPS. A. Crystal packing in the predominant *I*222 crystal form. Only one synthetase-glutaminase contact between tetramers is needed to build the lattice (cyan). B. Crystal contact of Asn395 and Asp404 (purple) on the non-conserved glutaminase loop (cyan). CTPS N395S/D404H was constructed. C. Non-conserved synthetase loops in crystal contact. CTPS/N395S/D404H crystallized isomorphously with wild type so Arg34, Arg268 and Asp404 (orange) at this contact were substituted.

Effect of GTP on the thermal stability of CTPS.

Based on sequence alignments, scanning alanine mutagenesis and limited proteolysis, two different regions on CTPS are implicated as the GTP binding site[116,118,119]. I considered two possibilities for GTP binding: either GTP binds to a single domain or a conformational shift brings the two regions together into a single GTP

binding site. In order to distinguish between these hypotheses, I tested the effect of individual substrates and combinations of substrates on the thermostability of the excised glutaminase domain and the full length CTPS. Constructs encoding an excised synthetase domain were also generated but the excised domain was insoluble. Full length CTPS unfolded outside the range of the instrument, so guanidinium chloride was used to shift the melting temperature (T_m) within the instrument range (Fig. 4.10A). All substrates and GTP had a stabilizing effect on CTPS, with UTP having the largest effect (Fig. 4.10B/C). Observed effects on the full-length protein are expected to be larger in the absence of a denaturing agent. Glutamine and GTP had little effect separately or together on the excised glutaminase domain (Fig. 4.10D/E). The effects of glutamine and GTP on the full-length protein, in contrast to their effects on the excised glutaminase domain, suggest that the glutaminase domain does not experience normal binding without the synthetase domain. These results do not eliminate the possibility that GTP binds solely to the glutaminase domain.

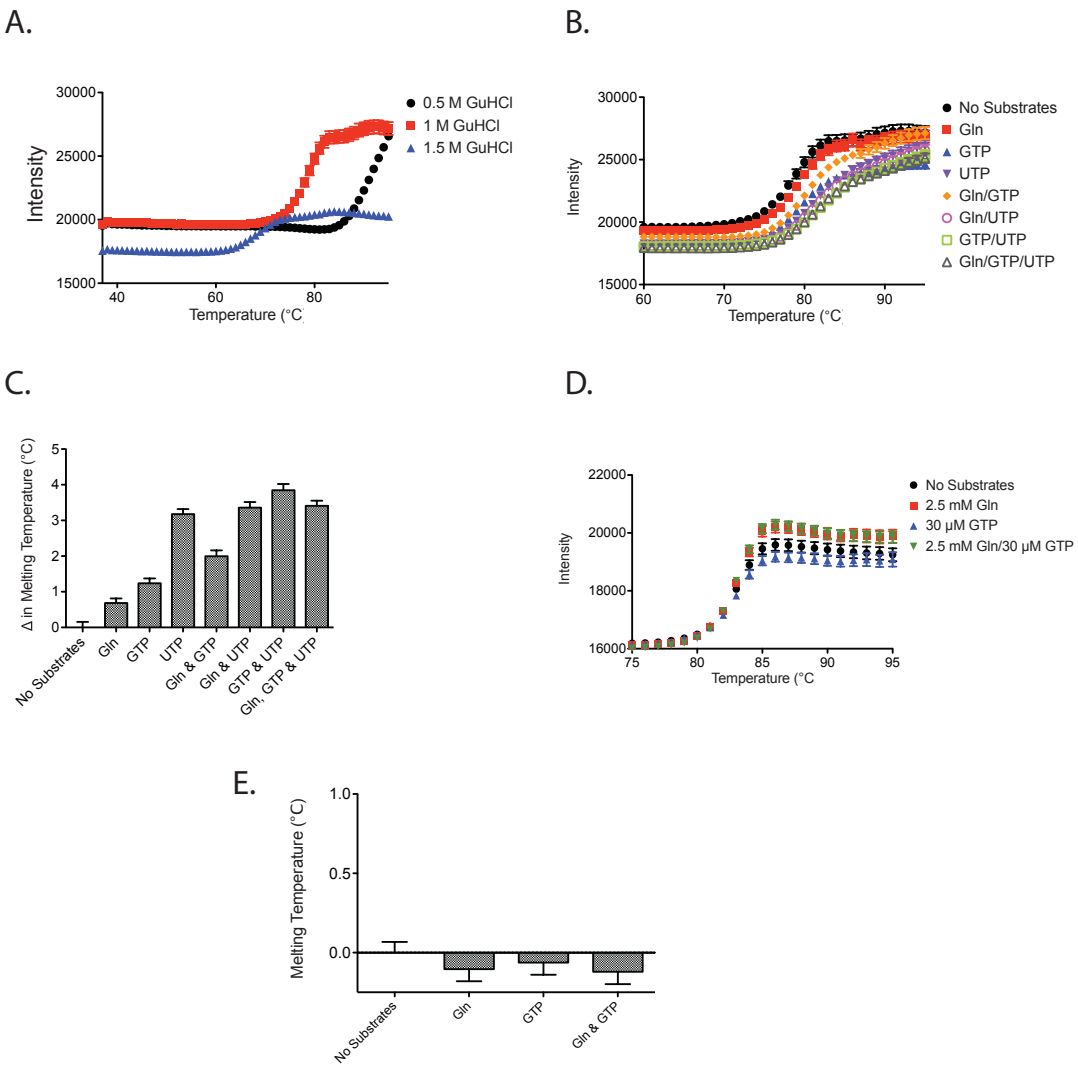

Figure 4.10 Effect of substrates and GTP on the thermal stability of Aa CTPS and the excised glutaminase domain. A. Effect of GuCl on CTPS Tm. 1.0 M GuCl was chosen to place the thermal transition within the operating range of the instrument. B. Melting curves for CTPS with substrates and GTP. C. Effect of substrates and GTP on CTPS T_m. D. Melting curves for the glutaminase domain with glutamine and GTP. E. Effect of glutamine or GTP on glutaminase domain T_m.

Solution structure studies on the effect of substrates on the CTPS tetramer.

In *Caulobacter crescentus* and *E. coli* cells CTPS was reported to form structural filaments[123]. Filament formation could be reconstituted *in vitro*, and was dependent on glutaminase activity and disrupted by DON[123]. The published experiments were

conducted in the presence GTP, glutamine, ATP, Mg^{+2} and UTP. Based on the reported dependence of the filament phenotype on glutaminase activity and the GTP enhancement of glutaminase activity, I hypothesized that understanding the filament structure may provide clues about the GTP binding site. I also wanted to test whether filament formation is dependent on GTP. With help from Dr. Georgios Skiniotis, we tested for filament formation using negative stain EM. However, under the published conditions filament formation for Aa CTPS was not observed. At this resolution I did not observe any large-scale conformational changes in the absence or presence of GTP or when DON was used instead of glutamine (Fig. 4.11).

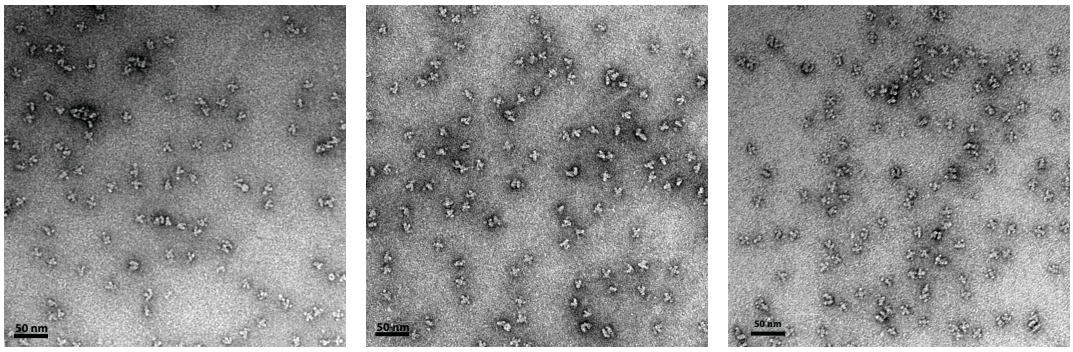

Figure 4.11 Negative stain EM images of Aa CTPS in the presence of various substrates.

Discussion

Despite the significant efforts to obtain the structure of a CTPS complex with GTP, I was unsuccessful. Previous workers proposed that GTP enhances the ability of CTPS to form the glutamyl thioester intermediate and I proposed that GTP does this by facilitating a large conformational change. The structural studies are not consistent with the interpretations of some biochemical results that DON occupies half of the

glutaminase active sites[115]. Based on the structure and biochemical analysis it is clear that DON can occupy all four sites simultaneously. The residues that interact with the Cys376-DON are similar to the interactions observed for glutamine in the *Thermus thermophiles HB8* (PDB: 1VCO) CTPS structure and for DON in the glutaminase domain of human CTPS2 structure (PDB: 2V4U)[87]. Based on these interactions it appears that the structure of CTPS with DON is a state that mimics some aspects of the glutamyl thioester intermediate. The CTPS/DON/UTP/GTP tetramer differs slightly from the substrate-bound and product-bound tetramers. Superposition of the A-subunits of the substrate-bound and product-bound structures results in an observed subunit displacement of 3.6°[77]. Including the structure of CTPS/DON/UTP/GTP in the superposition reveals an intermediate displacement (Fig. 4.12). This structural change does not account for the formation of an ammonia channel or explain where GTP binds or how GTP enhances the glutaminase activity.

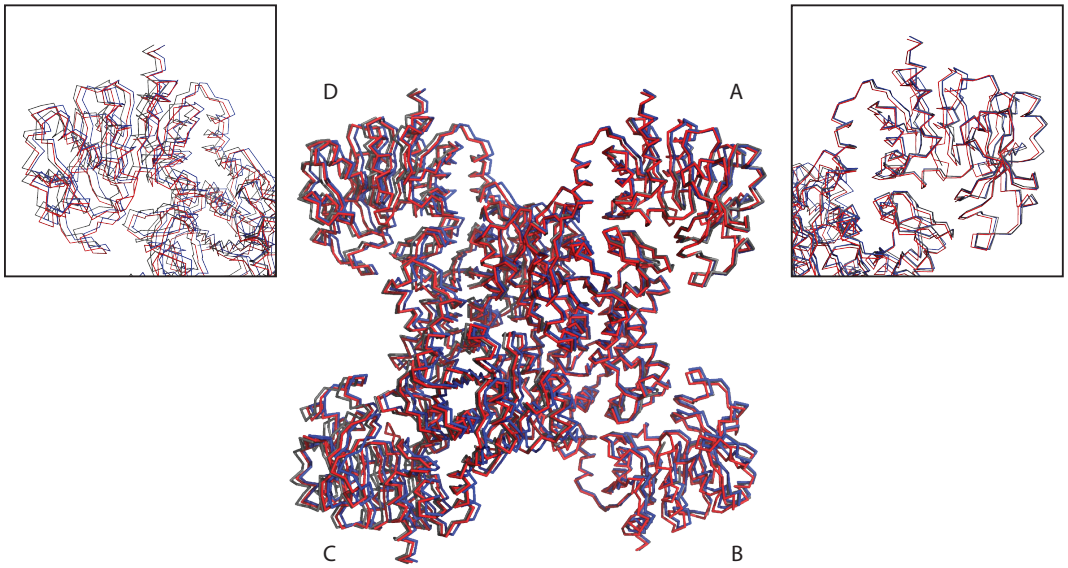

Figure 4.12 Comparison of the homotetramers of Aa CTPS nucleotide complexes. Alignment of chain A reveals that the overall tetramer changes depending on substrates bound (CTPS/UTP/ANP substrate complex (blue), CTPS/CTP/ADP product complex (gray) and CTPS/DON/UTP (red)).

The triphosphate density in the CTPS/DON/UTP/GTP map is that of GTP. The CTP and UTP binding sites overlap with respect to the triphosphate group (Fig. 4.13). The flexibility of this site to accommodate rotation of the ribose-base relative to the triphosphate would allow the GTP triphosphate to bind with the ribose and guanine disordered. If the triphosphate group were from UTP, the uracil and ribose density should be present in the identified UTP site. Additionally, a structure of CTPS modified with DON and co-crystallized with GTP was determined in order to eliminate the possibility that the triphosphate was that of UTP (Table 4.5). Density was present for a triphosphate group in both the previously identified ATP and UTP/CTP triphosphate sites. GTP was the only nucleotide present, supporting that GTP can bind to the other nucleotide binding sites (Fig. 4.14). The GTP concentration for activation is very narrow.

Concentrations greater than 0.15 mM slightly inhibit CTP synthesis without affecting glutamine hydrolysis, suggesting that GTP can bind to nucleotide sites other than its activating site[79]. Crystallization of substrate/effector complexes usually requires saturating concentrations. In this case this may have backfired. Although I was aware of this possibility, I was optimistic that GTP would bind in its native site in addition to potentially binding to other sites.

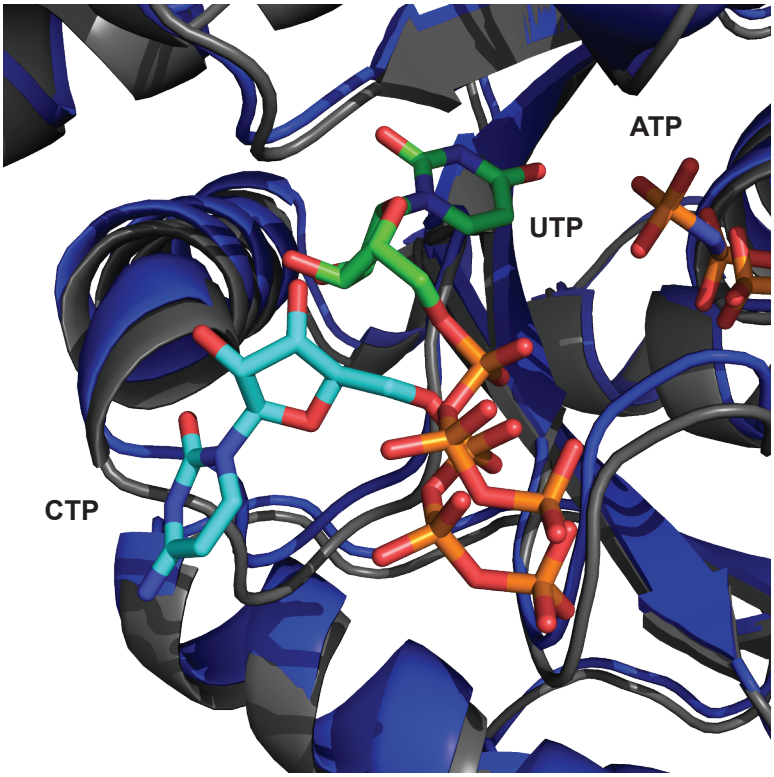

Figure 4.13 Overlapping UTP and CTP binding sites. UTP (Aa CTPS/UTP/ANP; blue, UTP; green sticks) binds in an orientation that points O4 towards ATP in preparation for activation. CTP (Aa CTPS/CTP/ADP; gray, CTP; cyan sticks) binds with the sugar and base away from the site of catalysis.

All structures of wild type Aa CTPS crystallize in the same space group regardless of the various combinations of substrates, co-factor and product. If the favorable crystal contacts are incompatible with a conformation with bound GTP, then disrupting the crystal contacts should escape the hurdle induced by crystallization.

Analysis of Aa CTPS in solution through transmission EM did not reveal any noticeable conformational changes. Although class averages were not obtained for the negative stain EM images, the overall cross shape of the homo-tetramer can be seen regardless of the substrates present. Furthermore, I observed very little thermal stabilization by GTP with either the full-length protein or the excised glutaminase domain. The results from my attempts suggest that the binding of GTP is neither strong nor induces a large conformation change to the overall architecture of CTPS.

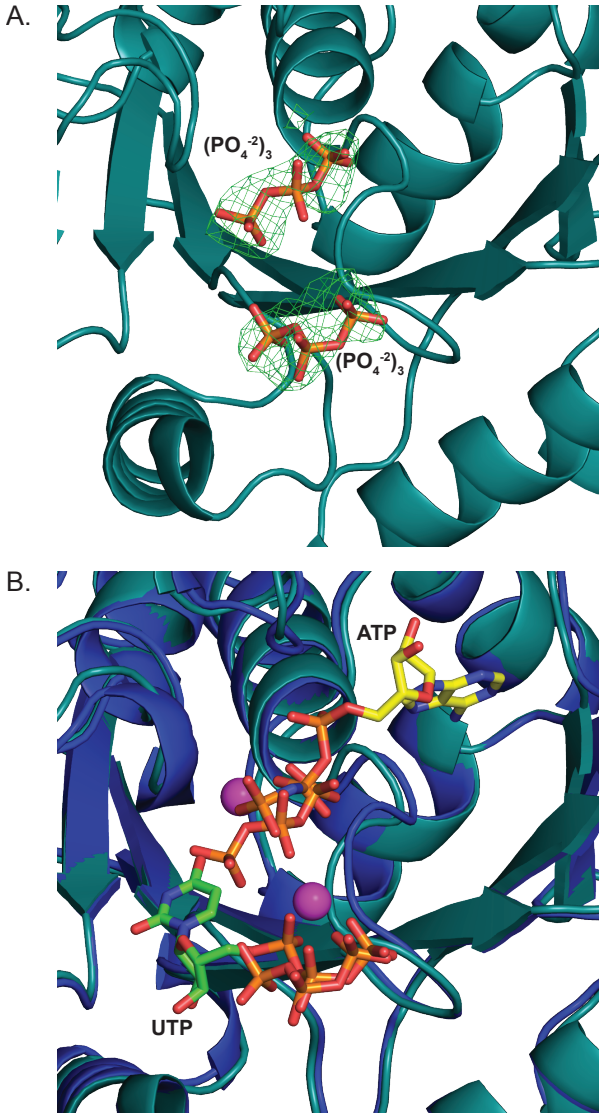

Figure 4.14 The GTP triphosphate binds to the identified ATP and UTP/CTP triphosphate sites. A. Triphosphate density is present in both the ATP and UTP/CTP triphosphate sites (green; F_o- F_c; omit density contoured at 3 σ). B. Superposition of CTPS/DON/GTP (teal) with the CTPS/UTP/ANP structure (blue) shows that triphosphate groups bind where the triphosphate group of ANP (yellow) is bound and a where the triphosphate group of UTP (green) is bound[77].

Chapter 5

Conclusions and Future Directions

This thesis concerns the structure-based mechanism of glutamine amidotransferases (GATs), which catalyze multi-step reactions. GATs are responsible for the coupled reaction of glutamine hydrolysis and amide transfer. The hydrolysis of glutamine to ammonia and glutamic acid occurs in the glutaminase active site. Ammonia is then transferred to the synthase active site without release to the bulk solvent. Although all GATs share the ability to hydrolyze glutamine and transfer the ammonia to a second active site located within the same protein/complex, their mechanisms and final products are diverse. The interest behind these enzymes lies in understanding how the two active sites are coordinated and how substrate binding influences mechanism.

Characterization of each known GAT further exemplifies the diversity of this group of enzymes. The differences between substrates, products and oligomeric state for each GAT trickle down into the differences between their mechanisms. Each GAT has a unique method to use glutamine and to synchronize bi-catalytic activity. The sole connection among the enzymes lies in the ability to hydrolyze glutamine. Understanding one GAT does not pave the way for understanding the entire group but does provide enlightenment on the many ways nature has evolved to utilize an efficient method for obtaining nitrogen, balancing metabolism and generating necessary small molecules.

Conclusions

PLP synthase (PLPS) is a single enzyme biosynthetic pathway for PLP from common metabolites. PLPS has separate glutaminase (PdxT) and synthase (PdxS) subunits that associate as a 24-mer ($PdxS_{12}PdxT_{12}$). Chapters 2 and 3 describe studies to understand details of the synthase catalytic activity. To investigate the mechanism of the synthase subunit and the role of the C-terminal tail of PdxS, I obtained three crystal structures of the synthase subunit alone (PdxS/R5P and PdxS/R5P/NH_3 complexes) or of the intact enzyme (PLPS/R5P/Gln). The structures provide snapshots of PdxS at distinct steps in its catalytic cycle and provide insights into the mechanism and structural elements that drive the conversion of the first amino ketone intermediate to the second chromophore intermediate. PdxS is highly dynamic, alternating between open and closed conformations depending on the presence of PdxT and substrates.

The complex of PLPS with its substrates, glutamine and R5P, is the first structure of intact PLPS with multiple substrates and visualization of the C-terminal tail. The C-terminal tail interacts with the body of the synthase subunit, acting as a lid over the R5P active site in the closed state of the synthase subunit. In absence of PdxT, formation of the amino ketone intermediate from R5P is not sufficient to close the PdxS active site in a manner similar to the intact PLPS structure with covalent adducts. Perturbations made to the closed conformation of PdxS affected chromophore formation. These results suggest that the closed conformation is necessary for chromophore formation.

The structure of PdxS with R5P unexpectedly contained a covalent modification at Lys149 with the phosphate group of 5RP bound to a secondary site outside the active

site. The attachment of 5RP C2 to Lys149 differs from the attachment of R5P C1 to Lys81, suggesting that the secondary phosphate site may be the site of G3P binding. Substitutions to residues that interact with the modified Lys149 affected either the two synthase activities chromophore formation and PLP synthesis or PLP synthesis alone. Substitutions to Lys149 also affected both synthase activities, suggesting that this residue plays a role in chromophore formation. The effect of Lys149 on chromophore formation contradicts the hypothesis that Lys149 and the secondary phosphate binding site are implicated in G3P binding. In the PLPS structure, the last ordered residue of the C-terminal tail (Gln290) binds to the secondary phosphate site. Therefore the C-terminal tail may not be able to bind to the PdxS core if this site were altered explaining why some substitutions around the secondary phosphate site affect chromophore formation. On the other hand, substitutions to either Glu103 or His115 solely affect PLP synthesis, suggesting that the secondary phosphate site also plays a role in G3P binding. The conformation of Lys149 appears to change in the presence of ammonia. In the PdxS/R5P/NH_3 structure Lys149 interacts with the chromophore inside the R5P active site, while in all other structures Lys149 resides outside of the active site. The flexibility of Lys149 and the dual role of the secondary phosphate-binding site supports a role in both chromophore formation and PLP synthesis.

The structure of PdxS with R5P in the presence of NH_3 captures three distinct states in the 12 active sites of the crystallographic asymmetric unit, providing snapshots of PdxS from amino ketone intermediate to chromophore intermediate. In all active sites a phosphate ion remains bound to the residues shared by the phosphate group of the amino ketone. Although helix α8' is 3 Å away from the R5P active site, an ordered water

molecule bridges the phosphate ion to this helix. Based on these results I propose a second potential binding site for G3P utilizing the same phosphate-binding site as R5P and the amino ketone intermediate. This hypothesis would suggest that the incorporation of G3P does not rely on catalytic assistance and therefore explains the lack of residues that are essential for PLP synthesis but not for chromophore formation.

Taken together the structures suggest that PdxS is dynamic, opening and closing depending on substrates bound and the association of subunits. I propose that PdxS is open before amino ketone formation and after chromophore formation. In the presence of PdxT, PdxS closes during the conversion of amino ketone to chromophore in anticipation of ammonia. Post chromophore formation, PdxS opens again in anticipation of G3P binding. The incorporation of G3P requires little or no catalytic assistance. I propose that Lys149 is the only residue that may play a role in G3P incorporation. Additionally, I propose that Lys149 plays a role in chromophore formation through interactions with the chromophore when inside the R5P active site. The secondary phosphate site is the region of PdxS where the C-terminal tail interacts with the core which is essential to chromophore formation and I propose that this site has a role in G3P binding. Overall, my studies have answered many questions while revealing many more.

Future Directions

Trapping G3P:

Based on my results, PdxS dynamics play a role in ensuring that the substrates bind in the right order. My hypothesis is that G3P binds only after the chromophore is formed and PdxS is in an open conformation. At this step, the presence of G3P would

lead to the formation of PLP. Crystallization of the synthase domain with bound G3P in the presence of the chromophore intermediate was not possible because I was unable to identify mutations that maintain chromophore formation while abolishing PLP synthesis. Additionally, chromophore instability also made it difficult to obtain a structure of the synthase subunit fully occupied with chromophore such that the G3P binding site might be identified. Based on the knowledge that I gained from the structures reported in Chapters 2 and 3, a stable unreactive chromophore mimic would be a great tool for trapping G3P. Incorporation of an unnatural amino acid that mimics the chromophore without facilitating turnover may allow for G3P to bind in crystals[124]. Additionally, the incorporation of an unnatural amino acid would generate a homogenous sample for crystallization mimicking the covalent complex. The covalent modification of the active site Lys81 with the chromophore makes using an unnatural amino acid a great tool. Although the structure of the chromophore is uncertain, an array of modified lysines are available in an unnatural amino acid library[125].

Characterization of the Lys149 adduct

Characterization of the synthase covalent intermediates (amino ketone and chromophore) has played a large role in understanding the mechanism of the synthase subunit of PLPS[56,57]. NMR experiments in combination with trapping reactions were used to identify the structure of both the amino ketone intermediate and the chromophore intermediate on Lys81[56,57]. Based on these structures, aspects of the mechanism were revealed and specific residues were probed around the active site as identified by crystal structures. NMR studies on the first covalent adduct revealed that it was an amino ketone and not a Schiff base as originally proposed[56]. This difference

explained the site of ammonia incorporation and, together with the structures described in the previous chapters, explained why Asp24 is critical to amino ketone formation.

Unexpectedly I also observed a covalent adduct at Lys149. Although it is unlikely that this covalent adduct participates in the catalytic pathway, determining the chemical structure of this adduct may shed light on this site's role. Based on the stability of the Lys149 adduct, I proposed that this adduct is not a Schiff base but an isoform of an initial C2 Schiff base. Refinement tests revealed that the 2-amino, 3-keto isomer at C2 (1-hydroxyl, 2-amino, 3-keto) was a better fit to the density on Lys149 than the alternative amino-ketone at C2 (1-al, 2-amino, 3-hydroxyl). Based on the chemical environment around the C3 ketone, the latter isoform is more likely than the former. Such would be consistent with the structure of G3P (C2 hydroxyl). If it is the amino ketone, this would be consistent with a possibility of G3P binding.

CTPS

Conclusions

CTP synthetase (CTPS) binds all four nucleotides: ATP and UTP substrates, CTP product, and GTP allosteric activator (UTP + ATP → CTP + ADP + P_i). Substrate binding is well established, as is the mechanism of product inhibition by CTP. I sought to understand allosteric activation by GTP, which may be involved with closing the gap between the glutaminase and synthetase active sites. Many methods were used in an attempt to capture a structure of CTPS with GTP. Based on previously published biochemical experiments, DON was used to mimic the glutamyl intermediate, mutagenesis was used to prevent predominant crystal contacts, domain excision was used to find the GTP binding site, and negative stain EM was used to observe the

protein in solution. Notably, the crystallization trials used saturating concentrations of GTP. Surprisingly, the triphosphate of GTP binds to the UTP/CTP and ATP triphosphate-binding sites but GTP is not observed elsewhere. This observation is consistent with studies that have shown that high GTP concentrations led to CTPS inhibition through the synthetase domain[79].

The results suggest that each nucleotide-binding site is not as discriminatory as expected based on the mechanism and kinetics of CTPS. The structure of CTPS/DON/UTP/GTP revealed that UTP could bind in the ATP binding site while the triphosphate group of GTP occupies the CTP/UTP site. The observation of density for a triphosphate group without density for either the ribose or guanine base is consistent with the density observed in the CTPS/DON/GTP structure that contained density for a triphosphate group in both the ATP triphosphate site and the UTP/CTP triphosphate site. Although, each nucleotide site excludes the ability of the ribose and guanine base to bind it does not exclude the ability for the triphosphate group to bind. This differs for UTP, which can bind to the ATP binding site. Overall the results are paradoxical to the importance of CTPS to regulate the balance of nucleotide levels in the cell.

Future Directions:

Characterizing the binding site of GTP

Many biochemical studies support the possibility of a large conformational change induced by the binding of GTP and the glutamyl intermediate. Although I did not observe these changes in solution or in crystal structures, without identifying the binding site of GTP the possibility cannot be ruled out. The structural requirements for activation

and binding for GTP have been tested using GTP analogs[117]. The results suggested that specific groups including those on the sugar, base and triphosphate group are critical for both binding and activation. Based on these results it is hypothesized that the entire molecule of GTP interacts with CTPS.

NMR would be a useful tool to test this interpretation. Labeled GTP is readily available commercially and can be used to measure the binding of GTP to CTPS through a handful of different NMR techniques (C^{13}, N^{15}, relaxation experiments, diffusion experiments, nuclear Overhauser effects)[126]. Preforming any or all of these experiments may reveal the change in environment that GTP experiences in the presence of CTPS and provide insights to the GTP binding site.

Solution structure analysis of CTPS in the presence of GTP

Although I did not observe a large conformational change for CTPS in the presence of various substrate combinations, GTP activation could occur through conformational changes that either bring the glutaminase domain closer to the synthetase domain and/or promotes the formation of the ammonia channel. The overall cross shape of CTPS may also allow for the glutaminase domain from one monomer to transfer its ammonia to the synthetase domain on another subunit, therefore the changes may not be as dramatic as I hypothesized. The rotational changes observed with different substrate combinations or crystallization conditions provide evidence that the domain interfaces are flexible[77,87]. Obtaining class averages for CTPS using either negative stain EM or cryo EM could provide insights into the conformational changes upon GTP binding.

Appendix I.

Sequence alignment of PdxS and 75 homologous sequences.

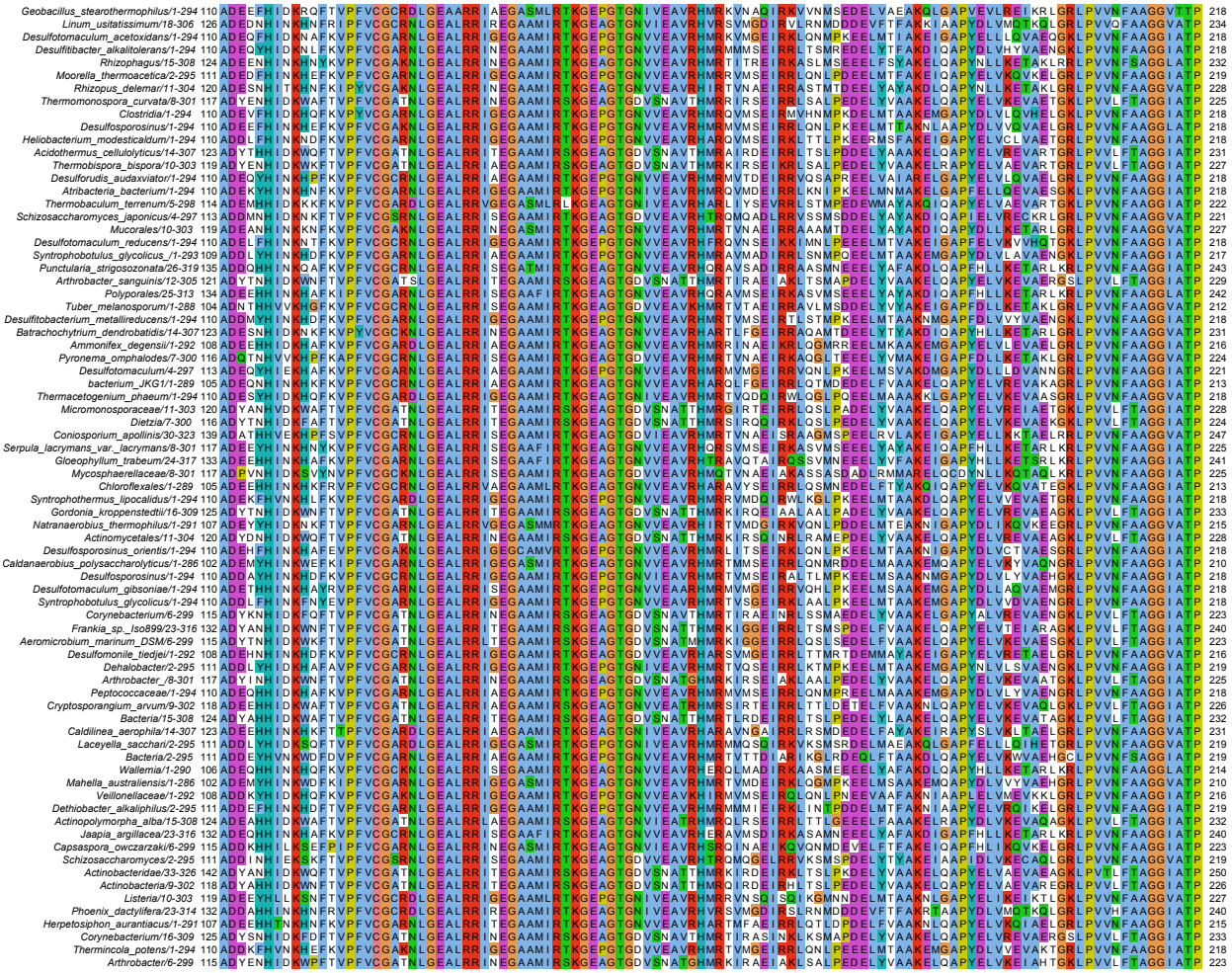
Geobacillus_stearothermophilus/1-294 110 ADEEFHIDKRQFTVPFVCGCRDLGEAARRIAEGASMLRTKGEPGTGNIVEAVRHMRKVNADIRKVVNMSEDELVAEAKQLGAPVEVLREIKRLGRLPVVNFAAGGVTTP 218
Linum_usitatissimum/18-306 126 ADEDNHINKHNFRIPFVCGCRNLGEALRRIREGAAMIRTKGEAGTGNVIEAVRHVRSVMGDIRVLRNMDDDEVFTFAKKIAAPYDLVMQTKQLGRLPVVQFAAGGVATP 234
Desulfotomaculum_acetoxidans/1-294 110 ADEQFHIDKNAFKVPFVCGARNLGEALRRIGEGAAMIRTKGEPGTGNVVEAVRHMRKVMGEIRKLQNMPKEELMTIAKEIQAPYELLLQVAEQGKLPVVNFAAGGIATP 218
Desulfitibacter_alkalitolerans/1-294 110 ADEQYHIDKNLFKVPFVCGARNLGEALRRINEGAAMIRTKGEPGTGNVVEAVRHMRMMMSEIRRLTSMREDELYTFAKDIQAPYDLVHYVAENGKLPVVNFAAGGIATP 218
Rhizophagus/15-308 124 ADEENHINKHNWKVPFVCGAKNLGEALRRINEGAAMIRTKGEAGTGNVVEAVRHMRTITREIRKASLMSEEELFSYAKELQAPYNLLKETAKLRRLPVVNFSAGGLATP 232
Moorella_thermoacetica/2-295 111 ADEDFHINKHEFKVPFVCGARNLGEALRRIGEGAAMIRTKGEPGTGNVVEAVRHMRRVMSEIRRLQNLPDEELMTFAKEIQAPYELVKQVKELGRLPVVNFAAGGIATP 219
Rhizopus_delemar/11-304 120 ADESNHITKHNFKIPYVCGAKNLGEALRRINEGAAMIRTKGEAGTGNVVEAVRHIRTVNAEIRRASTMTDEELYAYAKDLQAPYNLLKETAKLGRLPVVNFAAGGVATP 228
Thermomonospora_curvata/8-301 117 ADYENHIDKWAFTVPFVCGATNLGEALRRIREGAAMIRSKGEAGTGDVSNAVTHMRRIRSEIRRLSALPEDELYVAAKELQAPYELVKEVAETGKLPVVLFTAGGIATP 225
Clostridia/1-294 110 ADEVFHIDKHQFKVPYVCGARNLGEALRRIGEGAAMIRTKGEPGTGNVVEAVRHMRQVMSEIRMVHNMPKDELMTAAKEMGAPYDLVLQVHELGKLPVVNFAAGGIATP 218
Desulfosporosinus/1-294 110 ADEEFHINKHEFKVPFVCGAKNLGEALRRIGEGAAMIRTKGEAGTGNVVEAVRHMRMVMSEIRRLQNLPKEELMTTAKNLAAPYDLVVQVAELGRLPVVNFAAGGLATP 218
Heliobacterium_modesticaldum/1-294 110 ADDLFHINKNDFKVPFVCGARNLGEALRRIGEGAAMIRTKGEPGTGNVVEAVRHARQVMSEIRKLTTLPKEERMSFAKEIGAPYELVCLVAETGRLPVVNFAAGGIATP 218
Acidothermus_cellulolyticus/14-307 123 ADYTHHIDKWQFTVPFVCGATNLGEALRRITEGAAMIRSKGEAGTGDVSNAVTHMRAIRDEIRRLTSLPDDELYAAAKELQAPYELVREVARTGRLPVVLFTAGGIATP 231
Thermobispora_bispora/10-303 119 ADYENHIDKWKFTVPFVCGATNLGEALRRIAEGAAMIRSKGEAGTGDVSNAVTHMRKIRSEIRRLSALPEDELYVAAKELRAPYELVAEVARTGRLPVVLFTAGGIATP 227
Desulfurudis_audaxviator/1-294 110 ADEQYHINKHPFKVPFVCGARNLGEALRRIAEGAAMIRTKGEPGTGNVVEAVRHMRMVTDEIRRLVQSAPREELVAIARELGAPYELVLQVAELGRLPVVNFAAGGIATP 218
Atribacteria_bacterium/1-294 110 ADEKYHINKHNFKVPFVCGARNLGEALRRIGEGAAMIRTKGEPGTGNIVEAVRHMRQVMDEIRRLKNIPKEELMNMAKELGAPFELLQEVAESGKLPVVNFAAGGIATP 218
Thermobaculum_terrenum/5-298 114 ADEMHHIDKKKFKVPFVCGARDLGEALRRIVGEGASMLRLKGEAGTGNIVEAVRHARLIYSEVRRLSTMPEDEWMAYAQKIQAPYELVAEVARTGKLPVVNFAAGGIATP 222
Schizosaccharomyces_japonicus/4-297 113 ADDMNHIDKNKFTVPFVCGSRNLGEALRRISEGAAMIRTKGEAGTGDVVEAVRHTRQMQADLRRVSSMSDDELYAYAKDIQAPIELVRECKRLGRLPVVNFAAGGVATP 221
Mucorales/10-303 119 ADEEANHINKKNFKVPFVCGAKNLGEALRRINEGASMIRTKGEAGTGNVVEAVRHMRTVNAEIRRAAAMTDEELYAYAKDIQAPYDLLKETARLGRLPVVNFAAGGVATP 227
Desulfotomaculum_reducens/1-294 110 ADELFHINKNTFKVPFVCGCRNLGEALRRIGEGAAMIRTKGEPGTGNVVEAVRHFRQVNSEIKKIMNLPEEELMTVAKEIGAPFELVKVVHQTGKLPVVNFAAGGIATP 218
Syntrophobotulus_glycolicus_/1-293 109 ADDLYHINKHDFKVPFVCGARNLGEALRRIAEGAAMIRTKGEPGTGNVVEAVRHMRAVMADIRRLSNMPQEELMTAAKEMGAPYDLVLAVAENGKLPVVNFAAGGIATP 217
Punctularia_strigosozonata/26-319 135 ADDQHHINKQAFKVPFVCGCRNLGEALRRISEGAIMIRTKGEAGTGNVVEAVRHQRAVSADIRRASMNEEELYAFAKDLQAPFHLLKETARLKRLPVVNFAAGGLATP 243
Arthrobacter_sanguinis/12-305 121 ADYTNHIDKWNFTVPFVCGATSLGEALRRITEGAAMIRSKGEAGTGDVSNAITHMRTIRAEIAKLTSMAPDELYVAAKELQAPYELVKEVAERGSLPVVLFTAGGIATP 229
Polyporales/25-313 134 ADEEHHINKHAFKIPFVCGARNLGEALRRISEGAAFIRTKGEAGTGNVVEAVRHQRAVMSEIRKASVMSEEELYAYAKDIQAPFHLLKETARLKRLPVVNFAAGGLATP 242
Tuber_melanosporum/1-288 104 ADNTHHVVKHGFKVPFVCGCRNLGEALRRISEGAAMIRTKGEAGTGDVVEAVKHMRTVTAEIRRAVLMSDDELYVYAKEIGAPFDLLKETAKLGRLPVVNFAAGGVATP 212
Desulfitobacterium_metallireducens/1-294 110 ADDMYHINKHDFKVPFVCGARNLGEALRRIGEGAAMIRTKGEPGTGNVVEAVRHMRTVMSEIRTLSTMPKEELMTAAKNMGAPFDLVVYVAENGKLPVVNFAAGGIATP 218
Batrachochytrium_dendrobatidis/14-307 123 ADESNHIDKNKFKVPYVCGCKNLGEALRRINEGAAMIRTKGEAGTGNVVEAVRHARTLFGEIRRAQAMTDEELYTYAKDIQAPYHLLKETARLGRLPVVNFAAGGVATP 231
Ammonifex_degensii/1-292 108 ADEEHHIDKHAFKVPFVCGARDLGEALRRIAEGAAMIRTKGEAGTGNVVEAVRHMRRIRNAEIRRLQGMRREELMKAAKEMGAPYELVLEVAELGRLPVVNFAAGGIATP 216
Pyronema_omphalodes/7-300 116 ADGTNHVVKHPFKAPFVCGCRNLGEALRRISEGAAMIRTKGEAGTGDVVEAVRHMRTVNAEIRKAQGLTEEELYVMAKEIGAPFDLLKETAKLGRLPVVNFAAGGVATP 224
Desulfotomaculum/4-297 113 ADEQYHIEKHAFKVPFVCGARNLGEALRRIAEGAAMIRTKGEPGTGNVVEAVRHMRMVMGEIRRVQNLFKEELMSVAKDMGAPYDLLLDVANNGRLPVVNFAAGGVATP 221
bacterium_JKG1/1-289 105 ADEQNHIKHKFKVPFVCGCRNLGEALRRIAEGAAMIRTKGEAGTGNVVEAVRHARQLFGEIRRLQTMDEDELFVAAKELQAPYELVREVAKAGRLPVVNFAAGGIATP 213
Thermacetogenium_phaeum/1-294 110 ADESYHIDKQFKVPFVCGARDLGEALRRIGEGAAMIRTKGEAGTGNIVEAVRHMRTVQDQIRWLQGLPQEELMAAAKKLGAPYELVKEVAASGRLPVVNFAAGGVATP 218
Micromonosporaceae/11-303 120 ADYANHVDKWAFTVPFVCGATNLGEALRRITEGAAMIRSKGEAGTGDVSNAITTHMRGIRTEIRRLQSLPADELYVAAKELQAPYELVREIAETGKLPVVLFTAGGIATP 228
Dietzia/7-300 116 ADYTNHIDKFAFTVPFVCGATNLGEALRRITEGAAMIRSKGEAGTGDVSNAITTHMRSIRQDIRKLQSLPEDELYVAAKELQAPYELVKEVAEKGKLPVVLFTAGGIATP 224
Coniosporium_apollinis/30-323 139 ADATHHVEKHPFSVPFVCGCRNLGEALRRISEGAAMIRTKGEAGTGDVIEAVRHMRTVNAEISRAAGMSPEELRVLAKEIGAPYELLKKTAELRRLPVVNFAAGGVATP 247
Serpula_lacrymans_var_lacrymans/8-301 117 ADEEYHINKHNFKVPFVCGARNLGEALRRISEGAAFIRTKGEAGTGNVVEAVRHQRSVMSEIRKASVMSEEELYAYAKEIQAPFHLLKETARLKRLPVVNFAAGGIATP 225
Gloeophyllum_trabeum/24-317 133 ADEEHHINKHAFKVPFVCGARNLGEALRRISEGAAFIRTKGEAGTGNVVEAVRHTRAVQTAIRQSSVMNEEELYVFAKEIGAPYHLLKETSRLKRLPVVNFAAGGIATP 241
Mycosphaerellaceae/8-301 117 ADPVNHIDKSVNVPFVCGCKNLGEALRRISEGAAMIRTKGEAGTGDVVEAVRHMQTVNAEIAKASSASDADLRMMARELQCDVNLLKQTAQLKRLPVVNFAAGGIATP 225
Chloroflexales/1-289 105 ADEEHHINKHFRVPFVCGCRNLGEALRRVAEGAAMLRTKGEAGTGNVVEAVRHARAVYSEIRRLQSMNEDELFTYAKQIQAPYELVKQVATEGKLPVVNFAAGGIATP 213
Syntrophothermus_lipocalidus/1-294 110 ADEKFHVNKHLFKVPFVCGARDLGEALRRIGEGAAMIRTKGEPGTGNVVEAVRHMRRVMDQIRWLKGLPKEELMTAAKDLQAPYELVVEVAETGRLPVVNFAAGGIATP 218
Gordonia_kroppenstedtii/16-309 125 ADYTNHIDKWNFTVPFVCGATNLGEALRRITEGAAMIRSKGEAGTGDVSNAITTHMRKIRQEIAALAALPADELYVAAKELQAPYELVREVAEAGKLPVVLFTAGGIATP 233
Natranaerobius_thermophilus/1-291 107 ADEYYHIDKNKFTVPFVCGARNLGEALRRVGEGASMMRTKGEAGTGNVVEAVRHIRTVMDGIRKVQNLPDDELMTEAKNIGAPYDLIKQVKEEGRLPVVNFAAGGVATP 215
Actinomycetales/11-304 120 ADYDNHIDKWQFTVPFVCGATNLGEALRRINEGAAMIRSKGEAGTGDVSNAITTHMRKIRSDINRLRAMEPDELYVAAKELQAPYELVREVAEAGKLPVVLFTAGGIATP 228
Desulfosporosinus_orientis/1-294 110 ADEHFHINKHAFEVPFVCGAKNLGEALRRIGEGCAMVRTKGEPGTGNVVEAVRHMRLITSEIRKLQNLFKEELMTAAKNIGAPYDLVCTVAESGRLPVVNFAAGGIATP 218
Caldanaerobius_polysaccharolyticus/1-286 102 ADEMYHINKWEFKIPFVCGARNLGEALRRIGEGASMIRTKGEAGTGNVVEAVRHMRTMMSEIRRLQNMRDDELMAAAKEMQAPYELVKYVAQNGRLPVVNFAAGGIATP 210
Desulfosporosinus/1-294 110 ADDAYHINKHDFKVPFVCGCRNLGEALRRIGEGAAMIRTKGEPGTGNVIEAVRHMRTVMSEIRALTLMPKEELMSAAKNMGAPYDLVLYVAEHGKLPVVNFAAGGIATP 218
Desulfotomaculum_gibsoniae/1-294 110 ADETHHINKHAMRVPFVCGARNLGEALRRISEGAAMIRTKGEPGTGNVVEAARHMRMVMGEIRRVQHLPKEELMSAAKEMGAPYDLLADVAENGRLPVVNFAAGGIATP 218
Syntrophobotulus_glycolicus/1-294 110 ADDLFHINKFNVEVPFVCGARNLGEALRRIGEGAAMIRTKGEPGTGNVVEAVRHMRTVSGEIRKLAALPKEELMTAAKEMGAPYDLVVDVAENGRLPVVNFAAGGIATP 218
Corynebacterium/6-299 115 ADYKNHIDKFQFTVPFVCGATNLGEALRRINEGAAMIRSKGEAGTGDVSNAVTHMRTIRAEINRLSSMAEDELYAAKELGAPYALVREVAENGKLPVVLFTAGGIATP 223
Frankia_sp._Iso899/23-316 132 ADYANHIDKWNFTVPFVCGATNLGEALRRITEGAAMIRSKGEAGTGDVSNAITTHMRKIGGEIRRLTSMSPDELFVAAKELQAPYELVTEIARAGKLPVVLFTAGGIATP 240
Aeromicrobium_marinum_DSM/6-299 115 ADYTNHIDKWKFTVPFVCGATNLGEALRRLTEGAAMIRSKGEAGTGDVSNAIMHMRKIGGEIRRLQSLSEDELFVAAKELQAPYELVKEVAESGKLPVVLFTAGGIATP 223
Desulfomonile_tiedjei/1-292 108 ADEHNHINKHDFKVPFVCGCRNLGEALRRIGEGAAMIRTKGEAGTGDVVEAVRHARSVMGEIRRLTTMRTDEMMAYAKEIGAPYELVRETAELGRLPVVNFAAGGVATP 216
Dehalobacter/2-295 111 ADDLYHIDKHAFAVPFVCGARNLGEALRRIGEGAAMIRTKGEPGTGNIVEAVRHMRTVQSEIRRLKTMPKEELMTAAKEMGAPYNLVLSVAENGKLPVVNFAAGGIATP 219
Arthrobacter_/8-301 117 ADYINHIDKWNFTVPFVCGATNLGEALRRINEGAAMIRSKGEAGTGDVSNATGHMRKIRSEIAKLAALPEDELYVAAKELQAPYELVKEVAATGKLPVVLFTAGGIATP 225
Peptococcaceae/1-294 110 ADEQHHIDKHAFKVPFVCGARNLGEALRRIAEGAAMIRTKGEPGTGNVVEAVRHMRMVMSEIRRLQNMPREELMAAAKEMGAPYDLVLYVAENGRLPVVNFAAGGIATP 218
Cryptosporangium_arvum/9-302 118 ADEEHHIDKWAFTVPFVCGATNLGEALRRIAEGAAMIRSKGEAGTGNVVEATRHMRSIRTEIRRLTTLDETELFVAAKNLQAPYELVKEVAQLGKLPVVLFTAGGIATP 226
Bacteria/15-308 124 ADYAHHIDKWAFTVPFVCGATNLGEALRRITEGAAMIRSKGEAGTGDVSNAITTHMRTLRDEIRRLTSLPEDELYLAAKELQAPYELVKEVATAGKLPVVLFTAGGIATP 232
Caldilinea_aerophila/14-307 123 ADEEHHINKHKFTTPFVCGARDLGEALRRIAEGAAMIRTKGEAGTGNIVEAVRHARAVNGAIRRLRSMDEDELFAYAKEIRAPYSLVKLTAELGRLPVVNFAAGGVATP 231
Laceyella_sacchari/2-295 111 ADDLYHIDKSQFTVPFVCGARDLGEALRRIGEGASMIRTKGEPGTGNIVEAVRHMRMMQSQIRKVKSMSRDELMAEAKQLGAPFELLLQIHETGRLPVVNFAAGGVATP 219
Bacteria/2-295 111 ADDEYHVNKWDFDVPFVCGARNLGEALRRIAEGAAMIRTKGEPGTGNVVEAVRHMRTVTTDIARIKGLRDEQLFTAAKDLQAPYELVKWVAEHGCLPVVNFSAGGIATP 219
Wallemia/1-290 106 ADEQHHINKHQFKVPFVCGCKNLGEALRRISEGAAMIRTKGEAGTGNVVEAVRHERQLMADIRKAASMEEEELYAFAKDLQAPYHLLKETARLKRLPVVNFAAGGLATP 214
Mahella_australiensis/1-286 102 ADEMYHINKWDFKIPFVCGARNLGEALRRIGEGASMIRTKGEAGTGNVVEAVRHMRTVMDEIRKLQGMPKEELMSAAKEMQAPYDLVVYVAENGRLPVVNFAAGGIATP 210
Veillonellaceae/1-292 108 ADDKYHIDKHQFKVPFVCGARNLGEALRRIGEGAAMIRTKGEPGTGNVVEAVKHIRMVMSEIRQLQNLFNEEVAAFAKNIAAPLELVMEVKKLGRLPVVNFAAGGIATP 216
Dethiobacter_alkaliphilus/2-295 111 ADDEFHINKHDFTVPFVCGARNLGEALRRIGEGAAMIRTKGEPGTGNVVEAVRHMRMMMIEIRKLINTPDDELMTFAKNIAAPYELVRQIKELGRLPVVNFAAGGIATP 219
Actinopolymorpha_alba/15-308 124 ADEAHHIDKWAFTVPFVCGATNLGEALRRIAEGAAMIRSKGEAGTGNVIEATRHMRQLRSEIRRLTTLGEEELFAAAKELRAPYDLVKEVAAAGKLPVVLFTAGGIATP 232
Jaapia_argillacea/23-316 132 ADEQHHINKHAFKVPFVCGCRNLGEALRRINEGAAMIRTKGEAGTGNVVEAVRHERAVMSDIRKASAMNEEELYAFAKDIGAPFHLLKETARLKRLPVVNFAAGGIATP 240
Capsaspora_owczarzaki/6-299 115 ADDKHHILKSEFPIPVFCGARNLGEALRRINEGASMIRTKGEAGTGNVIEAVRHSRQINAEIKQVQNMDEVELFTFAKEIQAPYHLIKQVKELGRLPVVNFAAGGIATP 223
Schizosaccharomyces/2-295 111 ADDINHIEKSKFTVPFVCGSRNLGEALRRISEGAAMIRTKGEAGTGDVVEAVRHTRQMQGELRRVKSMSPDELYTYAKEIAAPIDLVKECAQLGRLPVVNFAAGGVATP 219
Actinobacteridae/33-326 142 ADYANHIDKWQFTVPFVCGATNLGEALRRITEGAAMIRSKGEAGTGDVSNATTHMRKIRDEIRKLTSLPKDELYVAAKELQAPYELVAEVAEAGKLPVTLFTAGGIATP 250
Actinobacteria/9-302 118 ADYAHHIDKWNFTVPFVCGATNLGEALRRITEGAAMIRSKGEAGTGDVSNAITTHMRQIRDEIRHLTSLPEDELYVAAKELQAPYELVAEVARERGLPVVLFTAGGIATP 226
Listeria/10-303 119 ADEEYHLLKSNFTVPFVCGCRDLGEALRRITEGAAMLRTKGEPGTGNIVEAVRHMRRVNSQISQIKGMNNDELMTIAKNLGAPYELIKEIKTLGRLPVVNFAAGGVATP 227
Phoenix_dactylifera/23-314 132 ADDAHHINKHNFRVPFVCGCRDLGEALRRIREGAAMIRTKGEAGTGNIVEAVRHVRSVMGDIRSLRNMDDDEVFTFAKRTAAPYDLVMQTKQLGRLPVVHFAAGGIATP 240
Herpetosiphon_aurantiacus/1-291 107 ADEEHHTNKHNFKVPFVCGARNLGEALRRIIEGAAMIRTKGEAGTGNVVEAVRHARTMFAEIRRLQTLDPDELFVAAKNLQAPYELVKEIAELGRLPVVNFAAGGIATP 215
Corynebacterium/16-309 125 ADYSNHIDKFDFTVPFVCGATNLGEALRRINEGAAMIRSKGEAGTGDVSNAVTHMRTIRASINKLKSMAPDELYVAAKELQAPYELVREVAERGSLPVVLFTAGGIATP 233
Thermincola_potens/1-294 110 ADDKFHVNKHEFKVPFVCGAKNLGEALRRIGEGAAMIRTKGEPGTGNVVEAVRHMRTVMGEIRRLQNLPEEELMTAAKEMGAPYDLVVEVAKTGRLPVVNFAAGGIATP 218
Arthrobacter/6-299 115 ADYENHIDKWPFTVPFVCGATNLGEALRRINEGAAMIRSKGEAGTGDVSNATGHMRKIRAEIAKLSALPEDELYVAAKELQAPYELVKEIAHTGKLPVVLFTAGGIATP 223

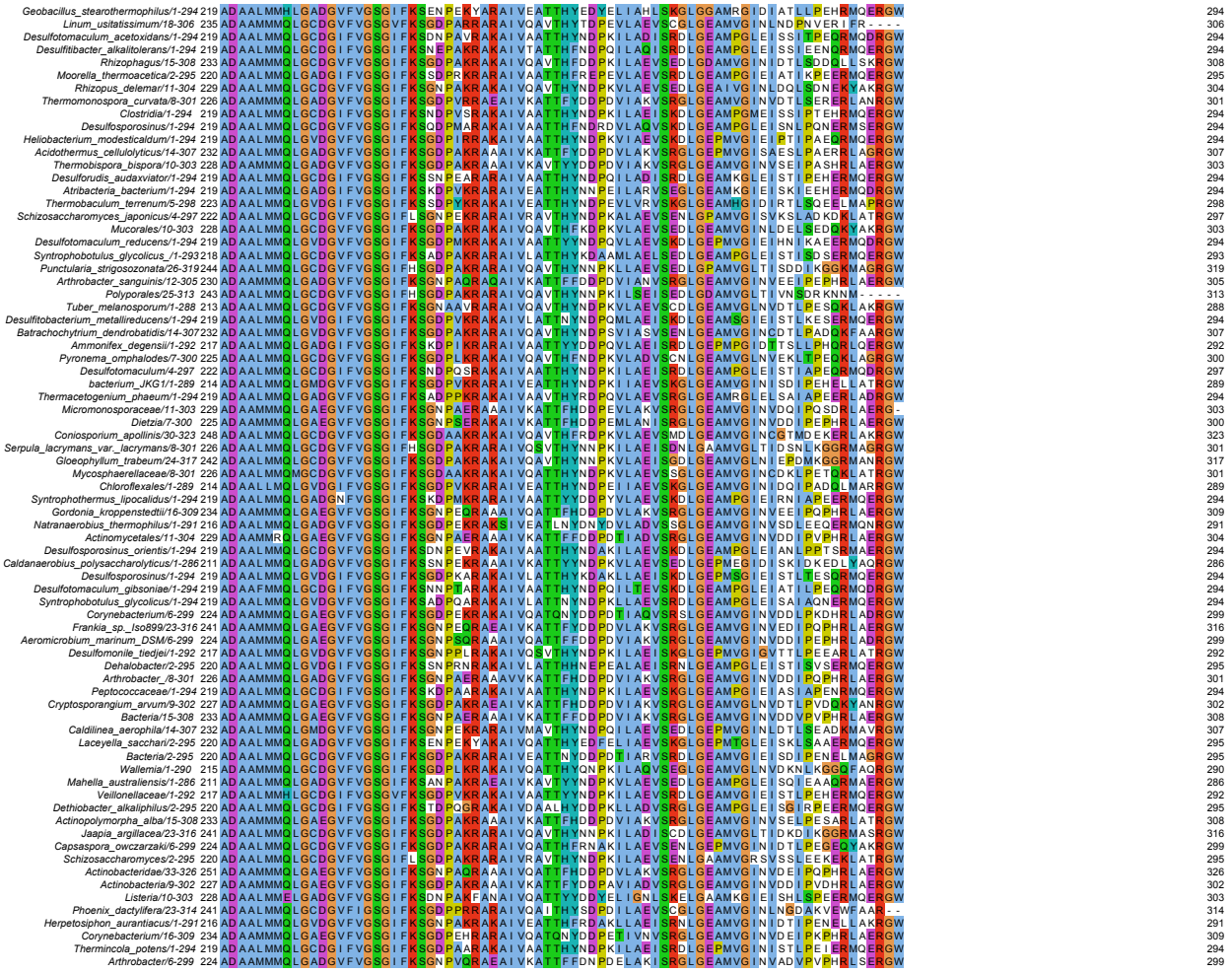

Alignment was generated using Consurf[127-129]. The search algorithm was CS-Blast and limited to 75 sequences. The color scheme is Clustal X[130,131].

References

1. Zalkin, H. & Smith, J.L. Enzymes utilizing glutamine as an amide donor. *Adv. Enzymol. Relat. Areas Mol. Biol.* **72**, 87-144 (1998).
2. Raushel, F.M., Thoden, J.B. & Holden, H.M. The amidotransferase family of enzymes: molecular machines for the production and delivery of ammonia. *Biochemistry* **38**, 7891-9 (1999).
3. Sonenshein, A.L. Control of key metabolic intersections in Bacillus subtilis. *Nat. Rev. Microbiol.* **5**, 917-27 (2007).
4. Chin, R.M., Fu, X., Pai, M.Y., Vergnes, L., Hwang, H., Deng, G., Diep, S., Lomenick, B., Meli, V.S., Monsalve, G.C., Hu, E., Whelan, S.A., Wang, J.X., Jung, G., Solis, G.M., Fazlollahi, F., Kaweeteerawat, C., Quach, A., Nili, M., Krall, A.S., Godwin, H.A., Chang, H.R., Faull, K.F., Guo, F., Jiang, M., Trauger, S.A., Saghatelian, A., Braas, D., Christofk, H.R., Clarke, C.F., Teitell, M.A., Petrascheck, M., Reue, K., Jung, M.E., Frand, A.R. & Huang, J. The metabolite alpha-ketoglutarate extends lifespan by inhibiting ATP synthase and TOR. *Nature* **510**, 397-401 (2014).
5. Mouilleron, S. & Golinelli-Pimpaneau, B. Conformational changes in ammonia-channeling glutamine amidotransferases. *Curr. Opin. Struct. Biol.* **17**, 653-64 (2007).
6. Raschle, T., Speziga, D., Kress, W., Moccand, C., Gehrig, P., Amrhein, N., Weber-Ban, E. & Fitzpatrick, T.B. Intersubunit cross-talk in pyridoxal 5'-phosphate synthase, coordinated by the C terminus of the synthase subunit. *J. Biol. Chem.* **284**, 7706-18 (2009).
7. Lewis, D.A. & Villafranca, J.J. Investigation of the mechanism of CTP synthetase using rapid quench and isotope partitioning methods. *Biochemistry* **28**, 8454-9 (1989).
8. Raschle, T., Amrhein, N. & Fitzpatrick, T.B. On the two components of pyridoxal 5'-phosphate synthase from Bacillus subtilis. *J. Biol. Chem.* **280**, 32291-300 (2005).
9. Strohmeier, M., Raschle, T., Mazurkiewicz, J., Rippe, K., Sinning, I., Fitzpatrick, T.B. & Tews, I. Structure of a bacterial pyridoxal 5'-phosphate synthase complex. *Proc. Natl. Acad. Sci. U. S. A.* **103**, 19284-9 (2006).
10. Tesmer, J.J., Klem, T.J., Deras, M.L., Davisson, V.J. & Smith, J.L. The crystal structure of GMP synthetase reveals a novel catalytic triad and is a structural paradigm for two enzyme families. *Nat. Struct. Biol.* **3**, 74-86 (1996).
11. Oinonen, C. & Rouvinen, J. Structural comparison of Ntn-hydrolases. *Protein Sci.* **9**, 2329-37 (2000).

12. Brannigan, J.A., Dodson, G., Duggleby, H.J., Moody, P.C., Smith, J.L., Tomchick, D.R. & Murzin, A.G. A protein catalytic framework with an N-terminal nucleophile is capable of self-activation. *Nature* **378**, 416-9 (1995).
13. Shin, S., Yun, Y.S., Koo, H.M., Kim, Y.S., Choi, K.Y. & Oh, B.H. Characterization of a novel Ser-cisSer-Lys catalytic triad in comparison with the classical Ser-His-Asp triad. *J. Biol. Chem.* **278**, 24937-43 (2003).
14. Chebrou, H., Bigey, F., Arnaud, A. & Galzy, P. Study of the amidase signature group. *Biochim. Biophys. Acta* **1298**, 285-93 (1996).
15. Mayaux, J.F., Cerbelaud, E., Soubrier, F., Yeh, P., Blanche, F. & Petre, D. Purification, cloning, and primary structure of a new enantiomer-selective amidase from a Rhodococcus strain: structural evidence for a conserved genetic coupling with nitrile hydratase. *J. Bacteriol.* **173**, 6694-704 (1991).
16. Neu, D., Lehmann, T., Elleuche, S. & Pollmann, S. Arabidopsis amidase 1, a member of the amidase signature family. *FEBS J* **274**, 3440-51 (2007).
17. Curnow, A.W., Hong, K., Yuan, R., Kim, S., Martins, O., Winkler, W., Henkin, T.M. & Soll, D. Glu-tRNAGln amidotransferase: a novel heterotrimeric enzyme required for correct decoding of glutamine codons during translation. *Proc. Natl. Acad. Sci. U. S. A.* **94**, 11819-26 (1997).
18. Nakamura, A., Yao, M., Chimnaronk, S., Sakai, N. & Tanaka, I. Ammonia channel couples glutaminase with transamidase reactions in GatCAB. *Science* **312**, 1954-8 (2006).
19. Pace, H.C. & Brenner, C. The nitrilase superfamily: classification, structure and function. *Genome Biol* **2**, REVIEWS0001 (2001).
20. Bellinzoni, M., De Rossi, E., Branzoni, M., Milano, A., Peverali, F.A., Rizzi, M. & Riccardi, G. Heterologous expression, purification, and enzymatic activity of Mycobacterium tuberculosis NAD(+) synthetase. *Protein Expr. Purif.* **25**, 547-57 (2002).
21. LaRonde-LeBlanc, N., Resto, M. & Gerratana, B. Regulation of active site coupling in glutamine-dependent NAD(+) synthetase. *Nat. Struct. Mol. Biol.* **16**, 421-9 (2009).
22. Christen, P. & Mehta, P.K. From cofactor to enzymes. The molecular evolution of pyridoxal-5'-phosphate-dependent enzymes. *Chem Rec* **1**, 436-47 (2001).
23. Eliot, A.C. & Kirsch, J.F. Pyridoxal phosphate enzymes: mechanistic, structural, and evolutionary considerations. *Annu. Rev. Biochem.* **73**, 383-415 (2004).
24. Hanada, K. Serine palmitoyltransferase, a key enzyme of sphingolipid metabolism. *Biochim. Biophys. Acta* **1632**, 16-30 (2003).
25. Percudani, R. & Peracchi, A. A genomic overview of pyridoxal-phosphate-dependent enzymes. *EMBO reports* **4**, 850-4 (2003).
26. Amadasi, A., Bertoldi, M., Contestabile, R., Bettati, S., Cellini, B., di Salvo, M.L., Borri-Voltattorni, C., Bossa, F. & Mozzarelli, A. Pyridoxal 5'-phosphate enzymes as targets for therapeutic agents. *Curr. Med. Chem.* **14**, 1291-324 (2007).
27. Livanova, N.B., Chebotareva, N.A., Eronina, T.B. & Kurganov, B.I. Pyridoxal 5'-phosphate as a catalytic and conformational cofactor of muscle glycogen phosphorylase B. *Biokhimiya/Biochemistry* **67**, 1089-98 (2002).

28. Kannan, K. & Jain, S.K. Effect of vitamin B6 on oxygen radicals, mitochondrial membrane potential, and lipid peroxidation in H2O2-treated U937 monocytes. *Free Radic. Biol. Med.* **36**, 423-8 (2004).
29. Bilski, P., Li, M.Y., Ehrenshaft, M., Daub, M.E. & Chignell, C.F. Vitamin B6 (pyridoxine) and its derivatives are efficient singlet oxygen quenchers and potential fungal antioxidants. *Photochem. Photobiol.* **71**, 129-34 (2000).
30. Jain, S.K. & Lim, G. Pyridoxine and pyridoxamine inhibits superoxide radicals and prevents lipid peroxidation, protein glycosylation, and (Na+ + K+)-ATPase activity reduction in high glucose-treated human erythrocytes. *Free Radical Biol. Med.* **30**, 232-7 (2001).
31. Ehrenshaft, M., Bilski, P., Li, M.Y., Chignell, C.F. & Daub, M.E. A highly conserved sequence is a novel gene involved in de novo vitamin B6 biosynthesis. *Proc. Natl. Acad. Sci. U. S. A.* **96**, 9374-8 (1999).
32. Ehrenshaft, M., Jenns, A.E., Chung, K.R. & Daub, M.E. SOR1, a gene required for photosensitizer and singlet oxygen resistance in Cercospora fungi, is highly conserved in divergent organisms. *Mol. Cell* **1**, 603-9 (1998).
33. Fitzpatrick, T.B., Amrhein, N., Kappes, B., Macheroux, P., Tews, I. & Raschle, T. Two independent routes of de novo vitamin B6 biosynthesis: not that different after all. *Biochem. J.* **407**, 1-13 (2007).
34. Galperin, M.Y. & Koonin, E.V. Sequence analysis of an exceptionally conserved operon suggests enzymes for a new link between histidine and purine biosynthesis. *Mol. Microbiol.* **24**, 443-5 (1997).
35. Ehrenshaft, M. & Daub, M.E. Isolation of PDX2, a second novel gene in the pyridoxine biosynthesis pathway of eukaryotes, archaebacteria, and a subset of eubacteria. *J. Bacteriol.* **183**, 3383-90 (2001).
36. Tazuya, K., Adachi, Y., Masuda, K., Yamada, K. & Kumaoka, H. Origin of the nitrogen atom of pyridoxine in Saccharomyces cerevisiae. *Biochim. Biophys. Acta* **1244**, 113-6 (1995).
37. Tanaka, K., Tazuya, K., Yamada, K. & Kumaoka, H. Biosynthesis of pyridoxine: origin of the nitrogen atom of pyridoxine in microorganisms. *J. Nutr. Sci. Vitaminol.* **46**, 55-7 (2000).
38. Zeidler, J., Gupta, R.N., Sayer, B.G. & Spenser, I.D. Biosynthesis of Vitamin B(6) in yeast. Incorporation pattern of trioses. *J. Org. Chem.* **68**, 3486-93 (2003).
39. Gupta, R.N., Hemscheidt, T., Sayer, B.G. & Spenser, I.D. Biosynthesis of vitamin B(6) in yeast: incorporation pattern of glucose. *J. Am. Chem. Soc.* **123**, 11353-9 (2001).
40. Burns, K.E., Xiang, Y., Kinsland, C.L., McLafferty, F.W. & Begley, T.P. Reconstitution and biochemical characterization of a new pyridoxal-5'-phosphate biosynthetic pathway. *J. Am. Chem. Soc.* **127**, 3682-3 (2005).
41. Bean, L.E., Dvorachek, W.H., Jr., Braun, E.L., Errett, A., Saenz, G.S., Giles, M.D., Werner-Washburne, M., Nelson, M.A. & Natvig, D.O. Analysis of the pdx-1 (snz-1/sno-1) region of the Neurospora crassa genome: correlation of pyridoxine-requiring phenotypes with mutations in two structural genes. *Genetics* **157**, 1067-75 (2001).

42. Osmani, A.H., May, G.S. & Osmani, S.A. The extremely conserved pyroA gene of Aspergillus nidulans is required for pyridoxine synthesis and is required indirectly for resistance to photosensitizers. *J. Biol. Chem.* **274**, 23565-9 (1999).
43. Rodriguez-Navarro, S., Llorente, B., Rodriguez-Manzaneque, M.T., Ramne, A., Uber, G., Marchesan, D., Dujon, B., Herrero, E., Sunnerhagen, P. & Perez-Ortin, J.E. Functional analysis of yeast gene families involved in metabolism of vitamins B1 and B6. *Yeast* **19**, 1261-76 (2002).
44. Seack, J., Perovic, S., Gamulin, V., Schroder, H.C., Beutelmann, P., Muller, I.M. & Muller, W.E. Identification of highly conserved genes: SNZ and SNO in the marine sponge Suberites domuncula: their gene structure and promoter activity in mammalian cells(1). *Biochim. Biophys. Acta* **1520**, 21-34 (2001).
45. Wrenger, C., Eschbach, M.L., Muller, I.B., Warnecke, D. & Walter, R.D. Analysis of the vitamin B6 biosynthesis pathway in the human malaria parasite Plasmodium falciparum. *J. Biol. Chem.* **280**, 5242-8 (2005).
46. Sakai, A., Kita, M., Katsuragi, T., Ogasawara, N. & Tani, Y. yaaD and yaaE are involved in vitamin B6 biosynthesis in Bacillus subtilis. *J. Biosci. Bioeng.* **93**, 309-12 (2002).
47. Gengenbacher, M., Fitzpatrick, T.B., Raschle, T., Flicker, K., Sinning, I., Muller, S., Macheroux, P., Tews, I. & Kappes, B. Vitamin B6 biosynthesis by the malaria parasite Plasmodium falciparum: biochemical and structural insights. *J. Biol. Chem.* **281**, 3633-41 (2006).
48. Zhu, J., Burgner, J.W., Harms, E., Belitsky, B.R. & Smith, J.L. A new arrangement of (beta/alpha)8 barrels in the synthase subunit of PLP synthase. *J. Biol. Chem.* **280**, 27914-23 (2005).
49. Zein, F., Zhang, Y., Kang, Y.N., Burns, K., Begley, T.P. & Ealick, S.E. Structural insights into the mechanism of the PLP synthase holoenzyme from Thermotoga maritima. *Biochemistry* **45**, 14609-20 (2006).
50. Zhang, X., Teng, Y.B., Liu, J.P., He, Y.X., Zhou, K., Chen, Y. & Zhou, C.Z. Structural insights into the catalytic mechanism of the yeast pyridoxal 5-phosphate synthase Snz1. *Biochem. J.* **432**, 445-50 (2010).
51. Guedez, G., Hipp, K., Windeisen, V., Derrer, B., Gengenbacher, M., Bottcher, B., Sinning, I., Kappes, B. & Tews, I. Assembly of the eukaryotic PLP-synthase complex from Plasmodium and activation of the Pdx1 enzyme. *Structure* **20**, 172-84 (2012).
52. Bauer, J.A., Bennett, E.M., Begley, T.P. & Ealick, S.E. Three-dimensional structure of YaaE from Bacillus subtilis, a glutaminase implicated in pyridoxal-5'-phosphate biosynthesis. *J. Biol. Chem.* **279**, 2704-11 (2004).
53. Belitsky, B.R. Physical and enzymological interaction of Bacillus subtilis proteins required for de novo pyridoxal 5'-phosphate biosynthesis. *J. Bacteriol.* **186**, 1191-6 (2004).
54. Hanes, J.W., Burns, K.E., Hilmey, D.G., Chatterjee, A., Dorrestein, P.C. & Begley, T.P. Mechanistic studies on pyridoxal phosphate synthase: the reaction pathway leading to a chromophoric intermediate. *J. Am. Chem. Soc.* **130**, 3043-52 (2008).
55. Raschle, T., Arigoni, D., Brunisholz, R., Rechsteiner, H., Amrhein, N. & Fitzpatrick, T.B. Reaction mechanism of pyridoxal 5'-phosphate synthase.

Detection of an enzyme-bound chromophoric intermediate. *J. Biol. Chem.* **282**, 6098-105 (2007).
56. Hanes, J.W., Keresztes, I. & Begley, T.P. 13C NMR snapshots of the complex reaction coordinate of pyridoxal phosphate synthase. *Nat. Chem. Biol.* **4**, 425-30 (2008).
57. Hanes, J.W., Keresztes, I. & Begley, T.P. Trapping of a chromophoric intermediate in the Pdx1-catalyzed biosynthesis of pyridoxal 5'-phosphate. *Angew. Chem.* **47**, 2102-5 (2008).
58. Kennedy, E.P. & Weiss, S.B. The function of cytidine coenzymes in the biosynthesis of phospholipides. *J. Biol. Chem.* **222**, 193-214 (1956).
59. Carter, J.R. & Kennedy, E.P. Enzymatic synthesis of cytidine diphosphate diglyceride. *J. Lipid Res.* **7**, 678-83 (1966).
60. Chang, Y.F. & Carman, G.M. CTP synthetase and its role in phospholipid synthesis in the yeast Saccharomyces cerevisiae. *Prog. Lipid Res.* **47**, 333-9 (2008).
61. Carman, G.M. & Henry, S.A. Phospholipid biosynthesis in yeast. *Annu. Rev. Biochem.* **58**, 635-69 (1989).
62. Verschuur, A.C., Van Gennip, A.H., Leen, R., Muller, E.J., Elzinga, L., Voute, P.A. & Van Kuilenburg, A.B. Cyclopentenyl cytosine inhibits cytidine triphosphate synthetase in paediatric acute non-lymphocytic leukaemia: a promising target for chemotherapy. *Eur. J. Cancer* **36**, 627-35 (2000).
63. Williams, J.C., Kizaki, H., Weber, G. & Morris, H.P. Increased CTP synthetase activity in cancer cells. *Nature* **271**, 71-3 (1978).
64. Warburg, O. On the origin of cancer cells. *Science* **123**, 309-14 (1956).
65. Lopez-Lazaro, M. The warburg effect: why and how do cancer cells activate glycolysis in the presence of oxygen? *Anticancer Agents Med Chem* **8**, 305-12 (2008).
66. Lieberman, I. Enzymatic amination of uridine triphosphate to cytidine triphosphate. *J. Biol. Chem.* **222**, 765-75 (1956).
67. Long, C.W. & Pardee, A.B. Cytidine triphosphate synthetase of Escherichia coli B. I. Purification and kinetics. *J. Biol. Chem.* **242**, 4715-21 (1967).
68. Hurlbert, R.B. & Kammen, H.O. Formation of Cytidine Nucleotides from Uridine Nucleotides by Soluble Mammalian Enzymes: Requirements for Glutamine and Guanosine Nucleotides. *J. Biol. Chem.* **235**, 443-449 (1960).
69. Chakraborty, K.P. & Hurlbert, R.B. Role of glutamine in the biosynthesis of cytidine nucleotides in Escherichia coli. *Biochim. Biophys. Acta* **47**, 607-9 (1961).
70. Kammen, H.O. & Hurlbert, R.B. Amination of uridine nucleotides to cytidine nucleotides by soluble mammalian enzymes; role of glutamine and guanosine nucleotides. *Biochim. Biophys. Acta* **30**, 195-6 (1958).
71. Levitzki, A. & Koshland, D.E., Jr. Role of an allosteric effector. Guanosine triphosphate activation in cytosine triphosphate synthetase. *Biochemistry* **11**, 241-6 (1972).
72. Long, C.W., Levitzki, A. & Koshland, D.E., Jr. The subunit structure and subunit interactions of cytidine triphosphate synthetase. *J. Biol. Chem.* **245**, 80-7 (1970).

73. Levitzki, A. & Koshland, D.E., Jr. Ligand-induced dimer-to-tetramer transformation in cytosine triphosphate synthetase. *Biochemistry* **11**, 247-53 (1972).
74. Koshland Jr, D.E. & Levitzki, A. *The Enzymes*, 1-866 (1974).
75. Pappas, A., Yang, W.L., Park, T.S. & Carman, G.M. Nucleotide-dependent tetramerization of CTP synthetase from Saccharomyces cerevisiae. *J. Biol. Chem.* **273**, 15954-60 (1998).
76. Levitzki, A. & Koshland, D.E., Jr. Cytidine triphosphate synthetase. Covalent intermediates and mechanisms of action. *Biochemistry* **10**, 3365-71 (1971).
77. V. Nagarajan, K.M.K., Etti Harms-Van Etten, Lee M. Graves and Janet L. Smith Structure and Activity of CTP Synthetase from an Extreme Thermophile. (Ann Arbor, 2009).
78. Bearne, S.L., Hekmat, O. & Macdonnell, J.E. Inhibition of Escherichia coli CTP synthase by glutamate gamma-semialdehyde and the role of the allosteric effector GTP in glutamine hydrolysis. *Biochem. J.* **356**, 223-32 (2001).
79. MacDonnell, J.E., Lunn, F.A. & Bearne, S.L. Inhibition of E. coli CTP synthase by the "positive" allosteric effector GTP. *Biochim. Biophys. Acta* **1699**, 213-20 (2004).
80. Endrizzi, J.A., Kim, H., Anderson, P.M. & Baldwin, E.P. Mechanisms of product feedback regulation and drug resistance in cytidine triphosphate synthetases from the structure of a CTP-inhibited complex. *Biochemistry* **44**, 13491-9 (2005).
81. Martin, E., Palmic, N., Sanquer, S., Lenoir, C., Hauck, F., Mongellaz, C., Fabrega, S., Nitschke, P., Esposti, M.D., Schwartzentruber, J., Taylor, N., Majewski, J., Jabado, N., Wynn, R.F., Picard, C., Fischer, A., Arkwright, P.D. & Latour, S. CTP synthase 1 deficiency in humans reveals its central role in lymphocyte proliferation. *Nature* **510**, 288-92 (2014).
82. Ozier-Kalogeropoulos, O., Fasiolo, F., Adeline, M.T., Collin, J. & Lacroute, F. Cloning, sequencing and characterization of the Saccharomyces cerevisiae URA7 gene encoding CTP synthetase. *Mol. Gen. Genet.* **231**, 7-16 (1991).
83. Ozier-Kalogeropoulos, O., Adeline, M.T., Yang, W.L., Carman, G.M. & Lacroute, F. Use of synthetic lethal mutants to clone and characterize a novel CTP synthetase gene in Saccharomyces cerevisiae. *Mol. Gen. Genet.* **242**, 431-9 (1994).
84. van Kuilenburg, A.B., Meinsma, R., Vreken, P., Waterham, H.R. & van Gennip, A.H. Isoforms of human CTP synthetase. *Adv. Exp. Med. Biol.* **486**, 257-61 (2000).
85. Weng, M., Makaroff, C.A. & Zalkin, H. Nucleotide sequence of Escherichia coli pyrG encoding CTP synthetase. *J. Biol. Chem.* **261**, 5568-74 (1986).
86. Endrizzi, J.A., Kim, H., Anderson, P.M. & Baldwin, E.P. Crystal structure of Escherichia coli cytidine triphosphate synthetase, a nucleotide-regulated glutamine amidotransferase/ATP-dependent amidoligase fusion protein and homologue of anticancer and antiparasitic drug targets. *Biochemistry* **43**, 6447-63 (2004).
87. Goto, M., Omi, R., Nakagawa, N., Miyahara, I. & Hirotsu, K. Crystal structures of CTP synthetase reveal ATP, UTP, and glutamine binding sites. *Structure* **12**, 1413-23 (2004).

88. Brosius, J., Erfle, M. & Storella, J. Spacing of the -10 and -35 regions in the tac promoter. Effect on its in vivo activity. *J. Biol. Chem.* **260**, 3539-41 (1985).
89. McCarthy, J.E., Schairer, H.U. & Sebald, W. Translational initiation frequency of atp genes from Escherichia coli: identification of an intercistronic sequence that enhances translation. *EMBO J.* **4**, 519-26 (1985).
90. Ringquist, S., Shinedling, S., Barrick, D., Green, L., Binkley, J., Stormo, G.D. & Gold, L. Translation initiation in Escherichia coli: sequences within the ribosome-binding site. *Mol. Microbiol.* **6**, 1219-29 (1992).
91. Minor, Z.O.a.W. Processing of X-ray Diffraction Data Collected in Oscillation Mode. . *Methods Enzymol.* **276**, 307-326 (1997).
92. McCoy, A.J., Grosse-Kunstleve, R.W., Adams, P.D., Winn, M.D., Storoni, L.C. & Read, R.J. Phaser crystallographic software. *J. Appl. Crystallogr.* **40**, 658-674 (2007).
93. McCoy, A.J. Solving structures of protein complexes by molecular replacement with Phaser. *Acta Crystallogr. Sect. D. Biol. Crystallogr.* **63**, 32-41 (2007).
94. Emsley, P. & Cowtan, K. Coot: model-building tools for molecular graphics. *Acta Crystallogr. Sect. D. Biol. Crystallogr.* **60**, 2126-32 (2004).
95. Winn, M.D., Ballard, C.C., Cowtan, K.D., Dodson, E.J., Emsley, P., Evans, P.R., Keegan, R.M., Krissinel, E.B., Leslie, A.G., McCoy, A., McNicholas, S.J., Murshudov, G.N., Pannu, N.S., Potterton, E.A., Powell, H.R., Read, R.J., Vagin, A. & Wilson, K.S. Overview of the CCP4 suite and current developments. *Acta Crystallogr. Sect. D. Biol. Crystallogr.* **67**, 235-42 (2011).
96. Merritt, J.P.a.E.A. TLSMD web server for the generation of multi-group TLS models. *J. Appl. Crystallogr.* **39**, 109-111 (2006).
97. Painter, J. & Merritt, E.A. Optimal description of a protein structure in terms of multiple groups undergoing TLS motion. *Acta Crystallogr. Sect. D. Biol. Crystallogr.* **62**, 439-50 (2006).
98. Lebedev, A.A., Young, P., Isupov, M.N., Moroz, O.V., Vagin, A.A. & Murshudov, G.N. JLigand: a graphical tool for the CCP4 template-restraint library. *Acta Crystallogr. Sect. D. Biol. Crystallogr.* **68**, 431-40 (2012).
99. Schuttelkopf, A.W. & van Aalten, D.M. PRODRG: a tool for high-throughput crystallography of protein-ligand complexes. *Acta Crystallogr. Sect. D. Biol. Crystallogr.* **60**, 1355-63 (2004).
100. O. S. Smart, T.O.W., A. Sharff, C. Flensburg, P. Keller, W. Paciorek, C. Vonrhein, and G. Bricogne. . Grade Server. v.1 101 edn (Global Phasing Ltd. , Cambridge, United Kingdom, 2011).
101. Chen, V.B., Arendall, W.B., 3rd, Headd, J.J., Keedy, D.A., Immormino, R.M., Kapral, G.J., Murray, L.W., Richardson, J.S. & Richardson, D.C. MolProbity: all-atom structure validation for macromolecular crystallography. *Acta Crystallogr. Sect. D. Biol. Crystallogr.* **66**, 12-21 (2010).
102. Moccand, C., Kaufmann, M. & Fitzpatrick, T.B. It takes two to tango: defining an essential second active site in pyridoxal 5'-phosphate synthase. *PLoS One* **6**, e16042 (2011).
103. Zhu, J. Purdue (2005).
104. Aslanidis, C. & de Jong, P.J. Ligation-independent cloning of PCR products (LIC-PCR). *Nucleic Acids Res* **18**, 6069-74 (1990).

105. Heras, B. & Martin, J.L. Post-crystallization treatments for improving diffraction quality of protein crystals. *Acta Crystallogr. Sect. D. Biol. Crystallogr.* **61**, 1173-80 (2005).
106. Long, F., Vagin, A.A., Young, P. & Murshudov, G.N. BALBES: a molecular-replacement pipeline. *Acta Crystallogr. Sect. D. Biol. Crystallogr.* **64**, 125-32 (2008).
107. Smart, O.S., Womack, T.O., Flensburg, C., Keller, P., Paciorek, W., Sharff, A., Vonrhein, C. & Bricogne, G. Exploiting structure similarity in refinement: automated NCS and target-structure restraints in BUSTER. *Acta Crystallogr. Sect. D. Biol. Crystallogr.* **68**, 368-80 (2012).
108. Nakamura, J., Straub, K., Wu, J. & Lou, L. The glutamine hydrolysis function of human GMP synthetase. Identification of an essential active site cysteine. *J. Biol. Chem.* **270**, 23450-5 (1995).
109. Klem, T.J. & Davisson, V.J. Imidazole glycerol phosphate synthase: the glutamine amidotransferase in histidine biosynthesis. *Biochemistry* **32**, 5177-86 (1993).
110. Bennett, B.D., Kimball, E.H., Gao, M., Osterhout, R., Van Dien, S.J. & Rabinowitz, J.D. Absolute metabolite concentrations and implied enzyme active site occupancy in Escherichia coli. *Nat. Chem. Biol.* **5**, 593-9 (2009).
111. Bhattacharya, M., Fuhrman, L., Ingram, A., Nickerson, K.W. & Conway, T. Single-run separation and detection of multiple metabolic intermediates by anion-exchange high-performance liquid chromatography and application to cell pool extracts prepared from Escherichia coli. *Anal. Biochem.* **232**, 98-106 (1995).
112. Jochmann, N., Gotker, S. & Tauch, A. Positive transcriptional control of the pyridoxal phosphate biosynthesis genes pdxST by the MocR-type regulator PdxR of Corynebacterium glutamicum ATCC 13032. *Microbiology* **157**, 77-88 (2011).
113. Goto, M., Omi, R., Miyahara, I., Hosono, A., Mizuguchi, H., Hayashi, H., Kagamiyama, H. & Hirotsu, K. Crystal structures of glutamine:phenylpyruvate aminotransferase from Thermus thermophilus HB8: induced fit and substrate recognition. *J. Biol. Chem.* **279**, 16518-25 (2004).
114. Kursula, P., Flodin, S., Ehn, M., Hammarstrom, M., Schuler, H., Nordlund, P. & Stenmark, P. Structure of the synthetase domain of human CTP synthetase, a target for anticancer therapy. *Acta Crystallogr. Sect. F. Struct. Biol. Cryst. Commun.* **62**, 613-7 (2006).
115. Levitzki, A., Stallcup, W.B. & Koshland, D.E., Jr. Half-of-the-sites reactivity and the conformational states of cytidine triphosphate synthetase. *Biochemistry* **10**, 3371-8 (1971).
116. Iyengar, A. & Bearne, S.L. Aspartate-107 and leucine-109 facilitate efficient coupling of glutamine hydrolysis to CTP synthesis by Escherichia coli CTP synthase. *Biochem. J.* **369**, 497-507 (2003).
117. Lunn, F.A., MacDonnell, J.E. & Bearne, S.L. Structural requirements for the activation of Escherichia coli CTP synthase by the allosteric effector GTP are stringent, but requirements for inhibition are lax. *J. Biol. Chem.* **283**, 2010-20 (2008).
118. Simard, D., Hewitt, K.A., Lunn, F., Iyengar, A. & Bearne, S.L. Limited proteolysis of Escherichia coli cytidine 5'-triphosphate synthase. Identification of residues

required for CTP formation and GTP-dependent activation of glutamine hydrolysis. *Eur. J. Biochem.* **270**, 2195-206 (2003).
119. Willemoes, M. Thr-431 and Arg-433 are part of a conserved sequence motif of the glutamine amidotransferase domain of CTP synthases and are involved in GTP activation of the Lactococcus lactis enzyme. *J. Biol. Chem.* **278**, 9407-11 (2003).
120. Leslie, A.W. & Powell, H. Processing diffraction data with mosflm.
121. Evans, P. Scaling and assessment of data quality. *Acta Crystallogr. Sect. D. Biol. Crystallogr.* **62**, 72-82 (2006).
122. Ohi, M., Li, Y., Cheng, Y. & Walz, T. Negative Staining and Image Classification - Powerful Tools in Modern Electron Microscopy. *Biol Proced Online* **6**, 23-34 (2004).
123. Ingerson-Mahar, M., Briegel, A., Werner, J.N., Jensen, G.J. & Gitai, Z. The metabolic enzyme CTP synthase forms cytoskeletal filaments. *Nat. Cell Biol.* **12**, 739-46 (2010).
124. Peeler, J.C. & Mehl, R.A. Site-specific incorporation of unnatural amino acids as probes for protein conformational changes. *Methods Mol. Biol.* **794**, 125-34 (2012).
125. Mehl, R.
126. Skinner, A.L. & Laurence, J.S. High-field solution NMR spectroscopy as a tool for assessing protein interactions with small molecule ligands. *J. Pharm. Sci.* **97**, 4670-95 (2008).
127. Ashkenazy, H., Erez, E., Martz, E., Pupko, T. & Ben-Tal, N. ConSurf 2010: calculating evolutionary conservation in sequence and structure of proteins and nucleic acids. *Nucleic Acids Res* **38**, W529-33 (2010).
128. Celniker, G., Nimrod, G., Ashkenazy, H., Glaser, F., Martz, E., Mayrose, I., Pupko, T. & Ben-Tal, N. ConSurf: Using Evolutionary Data to Raise Testable Hypotheses about Protein Function.
129. Berezin, C., Glaser, F., Rosenberg, J., Paz, I., Pupko, T., Fariselli, P., Casadio, R. & Ben-Tal, N. ConSeq: the identification of functionally and structurally important residues in protein sequences. *Bioinformatics* **20**, 1322-4 (2004).
130. Larkin, M.A., Blackshields, G., Brown, N.P., Chenna, R., McGettigan, P.A., McWilliam, H., Valentin, F., Wallace, I.M., Wilm, A., Lopez, R., Thompson, J.D., Gibson, T.J. & Higgins, D.G. Clustal W and Clustal X version 2.0. *Bioinformatics* **23**, 2947-8 (2007).
131. Goujon, M., McWilliam, H., Li, W., Valentin, F., Squizzato, S., Paern, J. & Lopez, R. A new bioinformatics analysis tools framework at EMBL-EBI. *Nucleic Acids Res.* **38**, W695-9 (2010).